

University of Alberta

Geometric Variations in Load-Bearing Joints

by

Kamrul Islam

A thesis submitted to the Faculty of Graduate Studies and Research
in partial fulfillment of the requirements for the degree of

Master of Science

in

Structural Engineering

Department of Civil and Environmental Engineering

©Kamrul Islam

Fall 2012

Edmonton, Alberta

Permission is hereby granted to the University of Alberta Libraries to reproduce single copies of this thesis and to lend or sell such copies for private, scholarly or scientific research purposes only. Where the thesis is converted to, or otherwise made available in digital form, the University of Alberta will advise potential users of the thesis of these terms.

The author reserves all other publication and other rights in association with the copyright in the thesis and, except as herein before provided, neither the thesis nor any substantial portion thereof may be printed or otherwise reproduced in any material form whatsoever without the author's prior written permission.

Dedication

Dedicated to my dad, A.F.M. Shamsul Islam, my mom, Shahina Akhter
Chowdhury, and my brother, Nazmul Islam

Abstract

The purpose of the current study was to investigate the geometric variations in the load-bearing joints among individuals. Two existing concepts in mathematics were introduced and their application in computational biomechanics was completely novel: 1) computing the depth of penetration between contact objects as an indirect measure of stress; and 2) computing the geometric similarity using the cubic root of volumetric ratio as a scaling law. Furthermore, an alternative geometric method to finite element analysis was proposed, which should be considered as a “proof of concept”.

This study demonstrated three novel results: 1) contrary to the current literature, the lateral aspect of the patellofemoral joint is not the sole indicator of PFPS; 2) the talus bones of the ankle joints are geometrically similar within a certain range of deviation; and 3) A standardized sizing for the talus bone implants which can fit all patients associated with traumatic talus bone injury.

Preface

This thesis is the result of two years research works since Fall 2010 under the supervision of Dr. Samer Adeeb and Dr. Kajsa Duke. This thesis is presented in an integrated article format. During the last two years, the following conference papers were published:

1. **Islam, K.**, Dobbe, A., Adeeb, S.M., El-Rich, M., Duke, K., Jomha, N.M. (2012), “Computer Methods for Designing Artificial Talus Bone in Ankle Joint”, Proceedings of the 36th Annual Meeting of the American Society of Biomechanics (ASB2012), August 15-18, 2012, Florida, USA.

2. **Islam, K.**, Mustafy, T., Adeeb, S.M., El-Rich, M., Ronsky, J.L. and Anderson, J. (2012), “A Novel Approach to Quantify Patellofemoral Joint Contact Stress”, Proceedings of the 18th Congress of the European Society of Biomechanics (ESB2012), July 1-4, 2012, Lisbon, Portugal.

3. Anderson, J., **Islam, K.**, Beaupre, L., Adeeb, S.M. (2012), “Three dimensional Computational Model for the study of Patellofemoral Biomechanics”, Proceedings of the 46th Canadian Orthopaedic Association/Canadian Orthopaedic Research Society (COA/CORS) Annual Meeting, June 8-10, 2012, Ottawa, Canada.

4. Mustafy, T., El-Rich, M., **Islam, K.**, Adeeb, S.M. (2012), “Finite Element Analysis of the Patellofemoral Joint Behavior under Frontal Impact”, Proceedings of the ASME-2012 Summer Bioengineering Conference, June 20-23, 2012, Fajardo, Puerto Rico, USA.

5. **Islam, K.**, Mustafy, T., Komeili, A., Adeeb, S.M., El-Rich, M., and Ronsky, J.L. (2012), “ Study of Contact Mechanisms in the PF joint of Normal versus PFPS subjects”, Proceedings of the 10th International Symposium of Computer Methods in Biomechanics and Biomedical Engineering, April 11-14, 2012, Berlin, Germany.

6. **Islam, K.**, Adeeb, S.M., El-Rich, M. and Ronsky, J.L. (2011), “On Estimating Penetration Depth of the Patellofemoral Joint”, Proceedings of the 12th Alberta BME Conference, October 22-24, 2011, The Banff Centre, Banff, Canada.

7. **Islam, K.**, Dobbe, A., Hajar, W., Duke, K., El-Rich, M., Adeeb, S., Jomha, N. (2012), “A Methodology for Designing Talar Prosthetics Based on Geometric Analysis”, submitted to the 13th Alberta BME Conference, October 19-21, 2012, The Banff Centre, Banff, Canada.

Acknowledgement

If I have the option not to write the acknowledgement part, I would better leave it. I really don't know how to express my feelings of the last two years. As I started, therefore, I have to finish, and this is really happening that I am finishing my M.Sc. Did I enjoy my last two years? Yes, it was amazing, full of fun, lots of anxiety, frustration, and uncertainties in various stages, but the people around Edmonton made my life beautiful, enjoyable and entertaining.

First, I would like to express my gratitude to my supervisor, Dr. Samer Adeeb. I did a lot of mistakes during the last two years. Sometimes you were upset, sometimes it made you angry, but you always forgot those, and in the next meeting I found you with a smiling face which I saw on the September 7, 2010 in our first meeting. You are one of the best persons I have ever seen in my entire life, and I am honoured to work with you. I went to Egypt in 2010, just one month before I came to Edmonton where you spent the first twenty four years of your life. You are an amazing person like the way I was amazed to see the incredible Egypt. Samer, you are a very good friend who tried to rectify me. You are the best supervisor who showed me how to think, how to come up with an idea, how to conduct research, how to face challenges, how to write, how to do constructive criticism, how to communicate professionally, how to supervise, how to behave, and above all, how to be a good person. I am not sure how much I am changed. But I am certain, I am not like what I was two years ago. Undoubtedly, I learnt a lot from your pleasant personality and attitude. Working with you was lot of fun without feeling pressures; otherwise, I won't be able to complete my research. I learnt how to conduct multi-task simultaneously as well as how to finish perfectly. I was a lecturer in an engineering university for eight months back home, and I had a different teaching philosophy. But closely seeing you in the last two years, it brought a lot of changes in my thoughts. Though I didn't agree with all of your techniques and philosophy of teaching, but I will try to follow you if I go to the academia in future. I am looking forward to working with you in future where ever I go.

I would like to thank my co-supervisor Dr. Kajsa Duke. Dr. Duke, though I worked with you for a short span, but it was very fruitful and pleasant. Most of the time you used to say, “Kamrul, work hard”. It was encouraging, and I really loved those words. I also would like to thank you for your enormous help to complete this research.

I would like to thank Dr. Marwan El-Rich for his constant guidance since 2011, and for being such a helpful person during my entire research. Besides my supervisors, I always found you, whenever I faced any problem in any stage. You always suggested me how to solve problems, and gave different directions which helped a lot in conducting the research.

I would like to thank my friends and lab mates for their constant support, inspirations and thoughtful ideas. I would also like to thank Mummad Mamun, my senior colleague, classmate and one of my best friend, for his helps, ideas, and supports in any situation. Mamun, you are more than a friend. I wish you all the best and there are lots of things to learn from you.

I would like to thank my family for their mental support throughout the entire M.Sc. Special thanks to my friend Md. Tazul Islam, Md. Hadiuzzaman, and his wife Tamanna Sarkar for their immense help and support during the last 2 years. I can't simply thank them enough. These three people were like my family, and I will never forget the support I got from them. It was because of Tazul, Hadi and Tamanna, I never felt that I was thousand miles away from my parents.

Finally, I would like to mention the names of few more people, Dr. Arman Ahmed, Dr. Hasan Zubayer, Dr. Nasrin Jahan, Dr. Mostafa Ali, Dr. Al-amin Khan Chowdhury, Ahsanul Karim Sohag, Abul Basar Baki, Masnuna Khatun, Rupak Mutsuddy, Md. Toihidul Islam, and Md. Nasiruddin, for making my stay in Edmonton beautiful and pleasant. I am really grateful for having such beautiful people around me.

Table of Contents

Dedication

Abstract

Preface

Acknowledgement

Table of Contents

Chapter 1	Introduction	1
	1.1 Background and Motivation	1
	1.2 Outline of the thesis	6
	1.3 References	7
Chapter 2	Study of Contact Mechanism in the PF Joint of Normal versus PFPS Subjects	11
	Paper I	12
Chapter 3	Three-Dimensional Geometric Analysis of the Talus for designing Talar Prosthetics	37
	Paper II	38
Chapter 4	Summary and Conclusions	63
	Biography	65

Chapter 1: Introduction

1.1 Background and Motivation

The word “Geometry” was devised from the ancient Egyptian and the Greek, signifying the division of land plots for tax purposes. Geometry literally means measurement of earth. From ancient through to modern times, geometry has had a profound effect as a basis in mathematics. While talking about the geometry, another two closely related terms, size and shape, are also important in a mathematical point of view.

Geometric analysis of simple shapes is well established in Mathematics. However, complex geometric shapes are difficult to define often resulting in a cumbersome analysis. Geometric shape analysis is very important in computational biomechanics. The human skeletal system is a fascinating structure comprised of complex joints. Each joint has a complex geometric shape as well varying in size. Each joint has its own characteristics and function based on location. Some joints are load-bearing, while others are non load-bearing in nature. Biomechanical engineers have been performing research to investigate the joint characteristics as early as the sixteenth century. However, still researchers are investigating the complex geometric shape of skeletal structures to explore new horizons.

Geometric shape of the musculo-skeletal system varies between individuals as differences in shape are related to biological growth. To identify the deviation of the geometric shape from the healthy normal geometry, is a prime concern of any biomechanical analysis. Injury, disease, or abnormal mechanical stimuli can aggravate the condition by changing the geometric shape. Computational modeling is a popular non-invasive technique to analyse complex geometric shapes. The mechanical behaviour of the particular biological system can be investigated by quantifying the mechanical stress, and observing the biological

growth, as well as comparisons of healthy versus symptomatic joints through geometric analysis.

In order to evaluate the geometric variations, two different but unique joints of human skeletal structure have been studied. One is the patellofemoral (PF) joint and the other is the ankle joint. Both of the joints are load-bearing and complex in shape. The goals of the current research work are two-fold: First, to apply engineering techniques to biological systems to create and analyse numerical models of musculoskeletal systems; and second, to develop non-invasive techniques for medical treatment to detect deviations from the norm and see the geometric variations between healthy and symptomatic joints.

Both the PF joint and the ankle joint experience large mechanical stress and motion during daily, as well as sports related activities. However, PF joints are the most injured areas compared to any human joint in orthopaedic biomechanics (Taunton et al. 2002). Besides the PF joint, the ankle joint is also a commonly injured area treated through orthopaedic surgery. Furthermore, ankle injuries due to sports are the most common pathologies for patients facing orthopaedic surgery (Anderson et al. 2011). Therefore, these two joints are of particular interest for orthopaedic biomechanics.

Numerous studies have described the anatomy and geometry of the PF joints and PF joint articular cartilage using various techniques. To describe the two opposing bony surfaces of a joint, the word congruency is frequently used, and defined as the similarity in the shape and geometry of the two surfaces (Ateshian et al. 1992). The PF joint is incongruous in nature (Hohe et al. 2002). A high degree of incongruity means greater joint stress which eventually leads to cartilage degeneration, patellofemoral pain syndrome (PFPS) and an early onset of osteoarthritis. Various researchers have described the articular surface geometry of the PF joints (Emery and Meachim 1973; Kwak et al. 1997; Wibeege 1941). However, few studies, to date, were conducted on congruency of PF joint

(Connolly et al. 2009a; b; Hohe et al. 2002; Kwak et al. 1997). Connolly et al. (2009b) quantified the in-vivo patellar tracking, geometry and mode of contact using MR imaging and compared healthy subjects with pathological subjects. Connolly et al. (2009a) also quantified the congruency of the PF joints using congruency index (CI) algorithm and proposed five modifications based on different surface representation to better understand the mode of contact and contact area in PF joints. Hohe et al. (2002) developed a quantitative analysis technique to determine surface size, curvature of the surface and joint congruency from in-vivo MRI. Joint congruency was determined from Gauss curvature analysis and surface areas were determined from 3D reconstruction process. Similarly, Kwak et al. (1997) qualified the articular cartilage surface of the PF joints using surface curvature analysis, and identified the topographic characteristics of the PF joint surface.

Various researchers used different techniques to define surface geometry of the PF joints. Ronsky et al. (1999) described a new non-contact method to determine cat PF joint contact surfaces using multistation digital photogrammetry (MDPG). Shih et al. (2004) also used photography to study the geometry of the femoral trochlear groove.

The etiology of the PF joint instability is still unclear. Attempts have been made by biomechanical researchers to describe the instability of PF joints and associated pathological consequences. Jafari et al. (2008) developed a 2D transverse plane computer model of the PF joint and investigated the effect of femoral groove geometry on patellar shift and tilt. Senavongse and Amis (2005) studied the effect of trochlear groove geometry on the stability characteristics of the PF joint. Berry et al. (2007) described that abnormal bony geometry, fibromuscular supports and neuromuscular control were the main biomechanical factors causing Patellofemoral pain syndrome (PFPS) as well as PF osteoarthritis. Amis (2007) described the functional characteristics and stability of the PF joint

from the anatomical point of view, and showed the influence of the patellar and trochlear surface geometry on the PF joint stability.

Mathematical models of generic PF joints were also used to qualify the mode of contact and to quantify the forces acting on the knee. Gill and O'Connor (1996) developed a 2D model of the PF joint using geometric and force equilibrium constraints, and showed the importance of incongruity in the geometry of the PF joint. Shahar and Banks-Sills (2004) proposed a 3D mathematical model of the canine knee to quantify the forces in the knee ligaments and the knee joint reaction forces during walking.

PF joint is a complex 3D structure. Researchers also developed finite element models to study the contact mechanics and stress distribution of PF joints (Besier et al. 2005, 2008; Farrokhi et al. 2011; Han et al. 2005).

Similar to the PF joints, the ankle joint is one of the major load-bearing and shock-absorbing joints of the musculo-skeletal system. The articular cartilage in the ankle joint is thinner compared to the knee, hip and PF cartilage. Restoration of proper ankle joint motion after severe ankle injuries is a challenging issue in orthopaedic surgery. Fusing, ankle bone replacement, ankle resurfacing, and total ankle replacement are all popular choices in ankle surgery for severely damaged ankles. However, inappropriate replacement of the ankle bone with a custom-made implant will result in abnormal ankle joint kinematics for the recovering patient. The anatomical structure of the ankle joint is very complex, and the structures involved are rather irregular in shape. The complete biomechanics of the ankle joint is not well established, unlike the cases of the hip and the knee joint mechanics. As such, it is important that a fuller understanding of the biomechanics of the ankle joint be reached. Numerous studies have been conducted to understand the biomechanics of the ankle joint and its associated instabilities (de Asla et al. 2006; Close 1956; Leardini 2001; Leardini et al. 1999a; b, 2000, 2001; Parr et al. 2012; Sheehan et al. 2007).

Although a fair amount of studies have been conducted to date on PF joints and ankle joints, confusion still exist regarding the contact mechanism and joint characteristics between healthy and symptomatic joints as well as their associated instabilities like PFPS and talus bone replacement through an implant. Therefore, a thorough understanding of the geometric shape variations in healthy and symptomatic joints is important. In most of the previous studies geometry holds the basis. Joint geometry plays an important role to maintain the health and functionality of the joint (Moskowitz 1992). Similarly, proper PF joint function depends on geometry (Moskowitz 1992). The load-bearing characteristics and joint contact mechanics depend on the geometric shape of the joint. Adeeb (2004) showed the effect of congruency on load-bearing joints, and investigated how the small variations in geometry could affect the contact stress and pressure distribution. Stress distribution over the cartilage surfaces also depends on geometric shape (Adeeb 2004; Donzelli et al. 1999; Eckstein et al. 1994, 1995; Stone and Yu 1997). Researchers have used finite element analysis for modelling and analysing the complex geometric shape of musculo-skeletal systems which exhibit highly complex interactions. FEA has risen in popularity as a numerical tool of choice to quantify contact stresses and areas which cannot be measured by direct mechanical test.

FEA is an approximate numerical technique to solve a boundary value problem. FEA is also an approximate method to solve the partial differential equation of equilibrium using weak formulation, where the entire problem is discretized into a finite number of elements. On each of these elements, the displacement is assumed to have a certain “shape” or form. The best approximation within the possible shapes is then obtained by minimizing an integral utilizing weak convergence. As it is an approximate method, therefore, the accuracy of the method can be achieved by increasing the element numbers, i.e., refining the mesh of the problem by increasing the number of elements. FEA is a viable tool not only to quantify the in-vivo joint contact stress and other mechanical stimuli,

but also to predict bone growth and bone remodeling, to assess the risk of fracture/failure of bone, and to design implants or prostheses.

To date, all the research work focused on the lateral aspect of the PF joint as a sole contributor of PFPS, and the current treatment strategy is strengthening the medial muscles to control the lateral shift of the patella. But recently some evidence was found that the medial shift of patella might cause PFPS. In that case, current treatment may be harmful for those individuals who have medial patellar maltracking.

At present, surgeons used to incorporate patient specific talus implant for talus bone replacement surgery. However, patient specific talus implant is not suitable due to various limitations in implant design and fixation system which has a long term detrimental effect on the patient as well as being very costly. To date, no such study has been performed for generalization of the talus implants that might be applicable to all patients associated with the talus injury.

In this study we developed computational modelling techniques utilizing the geometric shape of the joints to investigate the mechanical behaviour by observing the mechanical stress/deviation pattern, as well as comparisons of healthy versus symptomatic joints. Here we tackle two long standing problems of the orthopaedic biomechanics: 1) Investigation of the PFPS disease, and 2) Talus bone replacement through prosthetics. We propose an alternative geometric method to investigate the PFPS disease, and five different talus implants are also proposed based on certain criteria.

1.2 Outline of the Thesis

This thesis contains four chapters. Chapter 2 and 3 will be submitted to the scientific journal papers which were enclosed as **Paper I** and **Paper II**. Finally, summary and conclusions were discussed in Chapter 4.

1.3 References

- Adeeb, S. M. (2004). "Load-Bearing Across Diarthrodial Joints with special reference to peripheral structures and the menisci of the knee." Ph.D Thesis, University of Calgary, Calgary.
- Amis, A. A. (2007). "Current Concepts on Anatomy and Biomechanics of Patellar Stability." *Sports Medicine and Arthroscopy Review*, 15(2), 48–56.
- Anderson, D. D., Chubinskaya, S., Guilak, F., Martin, J. A., Oegema, T. R., Olson, S. A., and Buckwalter, J. A. (2011). "Post-traumatic osteoarthritis: Improved understanding and opportunities for early intervention." *Journal of Orthopaedic Research*, 29(6), 802–809.
- de Asla, R. J., Wan, L., Rubash, H. E., and Li, G. (2006). "Six DOF in vivo kinematics of the ankle joint complex: Application of a combined dual-orthogonal fluoroscopic and magnetic resonance imaging technique." *J. Orthop. Res.*, 24(5), 1019–1027.
- Ateshian, G. A., Rosenwasser, M. P., and Mow, V. C. (1992). "Curvature characteristics and congruence of the thumb carpometacarpal joint: differences between female and male joints." *J Biomech*, 25(6), 591–607.
- Berry, P. A., Teichtahl, A. J., Wluka, A. E., and Cicuttini, F. M. (2007). "The Role of Biomechanical Factors on Patellofemoral Osteoarthritis." *Current Rheumatology Reviews*, 3(2), 123–127.
- Besier, T. F., Gold, G. E., Beaupré, G. S., and Delp, S. L. (2005). "A modeling framework to estimate patellofemoral joint cartilage stress in vivo." *Med Sci Sports Exerc*, 37(11), 1924–1930.
- Besier, T. F., Gold, G. E., Delp, S. L., Fredericson, M., and Beaupré, G. S. (2008). "The influence of femoral internal and external rotation on cartilage stresses within the patellofemoral joint." *J. Orthop. Res.*, 26(12), 1627–1635.
- Close, J. R. (1956). "Some Applications of the Functional Anatomy of the Ankle Joint." *J Bone Joint Surg Am*, 38(4), 761–781.

- Connolly, K. D., Ronsky, J. L., Westover, L. M., Küpper, J. C., and Frayne, R. (2009a). "Analysis Techniques for Congruence of the Patellofemoral Joint." *Journal of Biomechanical Engineering*, 131(12), 124503.
- Connolly, K. D., Ronsky, J. L., Westover, L. M., Küpper, J. C., and Frayne, R. (2009b). "Differences in patellofemoral contact mechanics associated with patellofemoral pain syndrome." *Journal of Biomechanics*, 42(16), 2802–2807.
- Donzelli, P. S., Spilker, R. L., Ateshian, G. A., and Mow, V. C. (1999). "Contact analysis of biphasic transversely isotropic cartilage layers and correlations with tissue failure." *J Biomech*, 32(10), 1037–1047.
- Eckstein, F., Merz, B., Müller-Gerbl, M., Holzknicht, N., Pleier, M., and Putz, R. (1995). "Morphomechanics of the humero-ulnar joint: II. Concave incongruity determines the distribution of load and subchondral mineralization." *Anat. Rec.*, 243(3), 327–335.
- Eckstein, F., Merz, B., Schmid, P., and Putz, R. (1994). "The influence of geometry on the stress distribution in joints--a finite element analysis." *Anat. Embryol.*, 189(6), 545–552.
- Emery, I. H., and Meachim, G. (1973). "Surface morphology and topography of patello-femoral cartilage fibrillation in Liverpool necropsies." *J. Anat.*, 116(Pt 1), 103–120.
- Farrokhi, S., Keyak, J. H., and Powers, C. M. (2011). "Individuals with patellofemoral pain exhibit greater patellofemoral joint stress: a finite element analysis study." *Osteoarthr. Cartil.*, 19(3), 287–294.
- Gill, H., and O'Connor, J. (1996). "Biarticulating two-dimensional computer model of the human patellofemoral joint." *Clinical Biomechanics*, 11(2), 81–89.
- Han, S. K., Federico, S., Epstein, M., and Herzog, W. (2005). "An articular cartilage contact model based on real surface geometry." *Journal of biomechanics*, 38(1), 179–184.
- Hohe, J., Ateshian, G., Reiser, M., Englmeier, K.-H., and Eckstein, F. (2002). "Surface size, curvature analysis, and assessment of knee joint incongruity with MRI in vivo." *Magnetic Resonance in Medicine*, 47(3), 554–561.

- Jafari, A., Farahmand, F., and Meghdari, A. (2008). "The Effects of Trochlear Groove Geometry on Patellofemoral Joint Stability-a Computer Model Study." *Proceedings of the Institution of Mechanical Engineers, Part H: Journal of Engineering in Medicine*, 222(1), 75–88.
- Kwak, S. D., Colman, W. W., Ateshian, G. A., Grelsamer, R. P., Henry, J. H., and Mow, V. C. (1997). "Anatomy of the human patellofemoral joint articular cartilage: Surface curvature analysis." *Journal of Orthopaedic Research*, 15(3), 468–472.
- Leardini, A. (2001). "Geometry and mechanics of the human ankle complex and ankle prosthesis design." *Clinical Biomechanics*, 16(8), 706–709.
- Leardini, A., O'Connor, J. J., Catani, F., and Giannini, S. (1999a). "Kinematics of the human ankle complex in passive flexion; a single degree of freedom system." *Journal of Biomechanics*, 32(2), 111–118.
- Leardini, A., O'Connor, J. J., Catani, F., and Giannini, S. (1999b). "A geometric model of the human ankle joint." *Journal of Biomechanics*, 32(6), 585–591.
- Leardini, A., O'Connor, J. J., Catani, F., and Giannini, S. (2000). "The role of the passive structures in the mobility and stability of the human ankle joint: a literature review." *Foot Ankle Int*, 21(7), 602–615.
- Leardini, A., Stagni, R., and O'Connor, J. J. (2001). "Mobility of the subtalar joint in the intact ankle complex." *Journal of Biomechanics*, 34(6), 805–809.
- Moskowitz, R. W. (1992). *Osteoarthritis, diagnosis and medical/surgical management*. Saunders.
- Parr, H.J. Chatterjee, and C. Soligo. (2012). "Calculating the axes of rotation for the subtalar and talocrural joints using 3D bone reconstructions." *Journal of Biomechanics*, 45(6), 1103–1107.
- Ronsky, J. L., Boyd, S. K., Lichti, D. D., Chapman, M. A., and Šalkauskas, K. (1999). "Precise Measurement of Cat Patellofemoral Joint Surface Geometry With Multistation Digital Photogrammetry." *Journal of Biomechanical Engineering*, 121(2), 196.

- Senavongse, W., and Amis, A. A. (2005). "The effects of articular, retinacular, or muscular deficiencies on patellofemoral joint stability: a biomechanical study in vitro." *J Bone Joint Surg Br*, 87(4), 577–582.
- Shahar, R., and Banks-Sills, L. (2004). "A quasi-static three-dimensional, mathematical, three-body segment model of the canine knee." *Journal of Biomechanics*, 37(12), 1849–1859.
- Sheehan, F. T., Seisler, A. R., and Siegel, K. L. (2007). "In vivo talocrural and subtalar kinematics: a non-invasive 3D dynamic MRI study." *Foot Ankle Int*, 28(3), 323–335.
- Shih, Y.-F., Bull, A. M. J., and Amis, A. A. (2004). "The cartilaginous and osseous geometry of the femoral trochlear groove." *Knee Surgery, Sports Traumatology, Arthroscopy*, 12(4), 300–306.
- Stone, J. J., and Yu, H. (1997). "Computational contact analysis of joint congruency." *Biomed Sci Instrum*, 34, 368–373.
- Taunton, J. E., Ryan, M. B., Clement, D. B., McKenzie, D. C., Lloyd-Smith, D. R., and Zumbo, B. D. (2002). "A retrospective case-control analysis of 2002 running injuries." *Br J Sports Med*, 36(2), 95–101.
- Wibeeg, G. (1941). "Roentgenographs and Anatomic Studies on the Femoropatellar Joint: With Special Reference to Chondromalacia Patellae." *Acta Orthopaedica*, 12(1-4), 319–410.

Chapter 2: Study of Contact Mechanism in the PF Joint of Normal versus PFPS Subjects

A Journal Paper will be submitted to the Journal of Computer Methods in
Biomechanics and Biomedical Engineering:

This paper is presented in the next chapter with the title “**Paper I**”

Paper I

Study of Contact Mechanisms in the PF Joint of Normal versus PFPS Subjects

Kamrul Islam^a, Kajsa Duke^b, Tanvir Mustafy^a, Marwan El-Rich^a, Samer M. Adeeb^a and J.L. Ronsky^c

^aDepartment of Civil and Environmental Engineering, University of Alberta, Canada; ^bDepartment of Mechanical Engineering, University of Alberta, Canada; ^cDepartment of Mechanical and Manufacturing Engineering, University of Calgary, Canada

Corresponding Author:

Kamrul Islam
Department of Civil and Environmental Engineering
Markin/CNRL Natural Resources Engineering Facility
9105 116th St
Edmonton, Alberta, Canada
T6G 2W2

Phone: 1(780) 492 3718
Email: kamrul1@ualberta.ca

Abstract

The biomechanics of the patellofemoral (PF) joint is complex in nature, and the etiology of such manifestations of PF instability as patellofemoral pain syndrome (PFPS) is still unclear. Many experimental and numerical attempts have been made to investigate PFPS. In these attempts, abnormal stresses have often been cited as a prime cause of various instabilities in the PF joint, including PFPS. However, at this point the particular factors affecting PFPS have not yet been determined. The purpose of the present study is to develop computational models of the PF joint for the purpose of evaluating mechanical stimuli, such as stress. Magnetic Resonance Images (MRI) of healthy and PFPS subjects at knee flexion angles of 15°, 30°, and 45° during isometric loading have been used to develop the computational models. The present study has three objectives: the first is to develop three dimensional (3D) PF joint models using the finite element (FE) approach to quantify in-vivo cartilage contact stress; the second is to develop an alternative geometric method using a 3D registration technique and linear mapping to investigate the PF joint contact stress using an indirect measure: the depth of penetration of the patellar cartilage surface into the femur cartilage surface; and the third one is to compare the peak contact stress location (medial/lateral) obtained from the FE models with the location of the highest depth of penetration. The results obtained from both approaches demonstrated that the subjects with PFPS show higher contact stresses than the normal subjects. Maximum stress increases with flexion angle, and occurs in the lateral side in healthy and in the medial side in PFPS subjects. Based on the results obtained it has been concluded that the alternative geometric method is more robust and computationally efficient compared to FE analysis, and has the potential to assess PFPS with an accuracy similar to FE analysis.

Keywords: patellofemoral pain; cartilage; penetration depth; contact stress; finite element modeling

1. Introduction

The patellofemoral (PF) joint is one of the major load bearing joints, and research is currently being carried out to investigate the complex PF biomechanics in order to assess PF joint disorders. The PF joint is beginning to garner more attention in orthopaedic biomechanics due to such associated instabilities as patellar maltracking, chondromalacia of the patella, patellofemoral pain syndrome (PFPS), and patellar dislocation and subsequent initiation of osteoarthritis (OA). PFPS is one of the most common knee disorders, an ailment which affects more than 25% of the population (Devereaux and Lachmann 1984). Abnormal stresses are often cited as a primary cause of different instabilities in the PF joint, including PFPS. PFPS often affects people who are active and/or participate in sports (Fairbank et al. 1984; Fulkerson 2002a; Loud and Micheli 2001; Powers 2003). Numerous research programs have been undertaken in the past to investigate the PFPS. Despite what is known about this syndrome, though, it is still unclear what the exact cause of PFPS is (Fulkerson 2002a).

Patellar maltracking, which is associated with malalignment of the patella as well as an imbalance of the knee extensor muscles, is considered to be an important factor in the onset of PFPS (Ahmed et al. 1983; Cowan et al. 2009; Dhaher and Kahn 2002; Lee et al. 2002; Neptune et al. 2000; Powers et al. 1996; Sawatsky et al. 2012; Sheehan et al. 2009, 2012; Wilson et al. 2009). Muscle force imbalance results in a lateral shift of the patella, causing pain in the lateral side of the PF joint (Ahmed et al. 1983; Cowan et al. 2009; Dhaher and Kahn 2002; Lee et al. 2002; Powers et al. 1996; Sawatsky et al. 2012; Wilson et al. 2009). As such, the main clinical concern has been that patients with PFPS experience a higher load in the lateral facet of the PF joint. But, interestingly, a few recent studies have shown evidence of pain and cartilage wear in the medial side of the patellofemoral joint (Draper et al. 2012; Gorniak 2009; Song et al. 2011). This finding has constituted a clear contradiction of the previous reports discussing the PFPS. It should also be mentioned that elevated joint contact stresses are also considered to be a cause of PFPS (Fulkerson 2002b; Mach et al. 2002). Patients with patellofemoral pain also

experience an elevated level of bone metabolic activity at the PF joints, which is correlated with pain intensity (Draper et al. 2012).

In-vivo and in-vitro quantifications of PF joint contact stress were conducted using animal and cadaveric models (Ahmed et al. 1983; Huberti et al. 1984; Lee et al. 2003; Ronsky et al. 1995; Sawatsky et al. 2012). The lack of experimental measures coupled with the complexity of the joint have led researchers to develop finite element models of the PF joint in order to better understand the mechanism. Finite-element analysis (FEA) is the numerical tool of choice to quantify the joint contact stresses, as well as the areas which cannot be measured by means of direct mechanical tests. Researchers have developed finite element models to study the contact mechanics and stress distribution of PF joints (Besier et al. 2005, 2008; Elias et al. 2004; Farrokhi et al. 2011; Han et al. 2005). Previous finite element models of PF joints relied on muscle forces which were estimated from electromyographic (EMG) system which has many limitations

Estimation of penetration depth (PD) is conceptual and mathematical in nature. Several studies have defined and quantified PD in various ways (Fisher and Lin 2001; Ong 1997; Tang et al. 2009; Zhang et al. 2007). However, none of these studies have focused on using PD in computational biomechanics. Further details of the PD will be explained in the materials and methods section.

The primary goal of the present study is to develop an alternative geometric method using a 3D registration technique and linear mapping to investigate the PF joint contact stress using an indirect measure: the depth of penetration of the patellar cartilage surface into the femur cartilage surface. The secondary goal is to develop 3D FE models of the PF joint in order to quantify in-vivo cartilage contact stress. The novelty of this finite-element approach is the use of the registration technique and linear mapping to investigate the PF contact stresses, rather than using muscle forces. Finally, the study will compare the peak contact stress location (medial/lateral) obtained from the FE models with the location of highest depth of penetration.

2. Materials and methods

2.1 *Alternative Geometric Methods*

This study has used experimental data from 6 healthy (female, 26 ± 4 y, 167.0 ± 7.9 cm, 64.4 ± 5.7 kg) and 6 pathological (PFPS) subjects (female, 28 ± 8 y, 167.0 ± 4.7 cm, 59.0 ± 5.5 kg): All the subjects used in this study were female due to the significant difference in the knee joint kinematics between male and female subjects (Biscević et al. 2005; Csintalan et al. 2002; Malinzak et al. 2001). All subjects were scanned using 3.0 Tesla MR imaging at 15° , 30° , and 45° knee flexion angles. The MRI specifications and details about the subjects were given in Connolly (2006). A brief summary of the MRI specifications is described here.

The scanning was performed using a 3.0T MR imaging with the following specifications: repetition time: 17 ms; echo time: 3ms; flip angle: 90° ; image resolution: 0.625×0.625 mm², FOV: 16×16 cm², and slice thickness: 3mm.

The MRI machine software produced large number of sequential DICOM images of the experimental subject that were imported into the 3D image modelling software, MIMICS (Materialize NV, Belgium). Sagittal plane images were used to segment the patellofemoral joint surface, including cartilage boundaries, and the other two planes were utilized for better visualization of the full joint surface. 3D-reconstructed geometries of the patella and femur for 15° , 30° and 45° knee flexion angles were also created using MIMICS. The surfaces of the models were not smooth in texture However, in order to obtain an accurate cartilage surface geometry and thickness, no further smoothing of the models was completed.

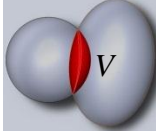
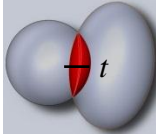
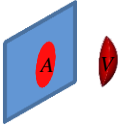
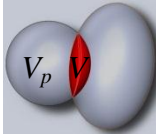
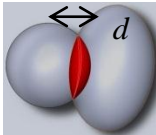
Following the digitization, two data sets of 3D geometry for the patella and femur (15° and 30° , 15° and 45°) were imported into the Geomagic Studio 12 (Raindrop Geomagic Inc.) at a time as the input for registration. The patella at the 15° position was chosen for the registration, whereas the femur is considered as a

fixed object in each case. Using the registration method, the patella at 15° is linearly transformed from its original position to weight-bearing positions (30° and 45°) in order to identify the complex interactions between the patella and femur surfaces. During the process of registration, in order to obtain the global coordinate transformation matrix, a common reference point is considered for the coordinate system of all sets of MRI data. The Centre of Gravity (CG) of the femur for the 15° knee flexion angle is considered as the reference point for the computational model coordinate system. The rigid registration method serves to align the patellar surface at the 15° position with the patellar surface at weight-bearing condition. This method of alignment is applicable to the rigid transformation of an object with 6 degrees of freedom (DOF) in 3D space (3 translations and 3 rotations). A transformation matrix that effectively maps these two objects can be easily obtained using the Geomagic Studio 12 software. The registration method is automatically checked by Geomagic Studio for symmetry, fine adjustment, and automatic deviator elimination with an estimation of average error, i.e., the average deviation of all points of comparison. (In this process, the smaller the value of error, the more precise the alignment is.) Then, the float surface is fitted to the fixed surface geometry. Finally, the rigid registration method is implemented by translating the non-weight-bearing patella to the CG of the weight-bearing patella and rotating the patellar surface twice by the rotation matrices (Stammberger et al. 2000).

The proximal relationship between the patella and femur is pertinent to the patellofemoral joint stability investigation. In this study, following the incorporation of the registration technique, the patellar surface (i.e., patella that was previously at 15° position) intersects the surface of the flexion femur (i.e., femur at 30° and 45° position). In this case, depth of penetration (PD) becomes the measure of proximity as the two objects (patella and femur) intersect one another virtually. Here, a novel and robust technique was developed in order to quantify the PD of the patellar surface to the femur surface as an indirect measure of stress. Abnormal patellofemoral stress patterns and alterations in the peak

stress location are considered the primary factors which contribute to PFPS. To the best of the researchers' knowledge, this study constitutes the first attempt to quantify stress in terms of PD in computational biomechanics research. In the present study, the virtual PD represents the indirect measure of the PF joint contact deformation. We measured PD using five different methods, and the PD has been defined as (a) PD₁: cubic root of intersection volume; (b) PD₂: highest thickness of intersection, (c) PD₃: ratio of the intersection volume to the projected surface area in contact, (d) PD₄: ratio of the intersection volume to the total volume of patella (non-dimensional); and (e) PD₅: shortest translational distance required which brings two objects in contact. We adopt a modified approach, similar to that explained in the refs. Ong (1997) and Fisher and Lin (2001). Among the five methods, only PD₂ has been used to evaluate the difference between medial and lateral side of the PF joint. Table 1 shows the details of the five different methods used in this study.

Table 1: Five different methods for quantifying PD

Method	Formula	Unit	Schematic Diagram
PD ₁	$\sqrt[3]{V^3}$	$\sqrt[3]{mm^3}$	
PD ₂	t	mm	
PD ₃	$\frac{V}{A}$	$\frac{mm^3}{mm^2}$	
PD ₄	$\frac{V}{V_p}$	$\frac{mm}{mm}$	
PD ₅	d	mm	

2.2 Finite Element Modeling

Computational modelling is gaining popularity in biomechanical research due to its flexibility and manipulating capacity for joint modelling. Complex joint characteristics and contact mechanics can easily be investigated through computational models. In-vivo joint stress cannot be measured using direct mechanical tests. Computational modelling, such as finite element method can be readily used to quantify stress/strain within the joints.

The geometry of the bony structures and soft tissues in this study were obtained following the procedures described in the previous section. In order to obtain smoothed surfaces for FEA, the binary STL file generated in MIMICS was imported into Geomagic Studio 12. After further refinement of the 3D geometry,

a similar registration technique to the one explained above was employed. The purpose of the registration technique is to use the undeformed patella (i.e., patella at 15° position), since the cartilage on the patella surface at the 30° and 45° positions is assumed to be already deformed with respect to the patella at 15° position. Finally, the non-uniform b-spline surfaces produced by Geomagic were exported to the IGS format, and the refined 3D PF joint geometry was imported into Hypermesh (Altair Engineering Inc., Troy, MI). FE meshes of the 3D-digitized models of the femur, patella, patellar cartilage, and femur cartilage were created using HyperMesh. The articular cartilage of the patella and femur were modeled as homogeneous isotropic tetrahedral elements with a modulus of elasticity of 12.0 MPa and a Poisson ratio of 0.45 (Mesfar and Shirazi-Adl 2005), whereas the femur and patella were modeled using shell elements. As we are not interested in fluid exudation and matrix consolidation, therefore, modeling the cartilage as linear elastic is sufficient to capture the in-vivo mechanical behavior of cartilage. Surface-to-surface contact was assumed based on the hard contact constraint, and the default penalty method was used for simulations using ABAQUS 6.10 (Simulia, Providence, RI). A very low coefficient of friction of 0.002 was assumed for the contact modelling (Adeeb 2004). For all simulations, the femur was constrained in all six degrees of freedom at the proximal end. Following application of the registration technique, it should be noted, the patellar surface virtually intersects the femur surfaces. Moreover, prior to initiation of the simulations, the patella was moved in the anterior direction to separate the both objects (i.e., femur and patella) from each other. This same amount of displacement was applied as a displacement controlled loading. All the finite element models were developed for left knee of one healthy and one PFPS subject for 30° and 45° knee position. Figure 1 depicts the modeling approach followed in this study to quantify mechanical stimulus (such as PD and stress), and figure 2 depicts meshed 3D model of PF joint.

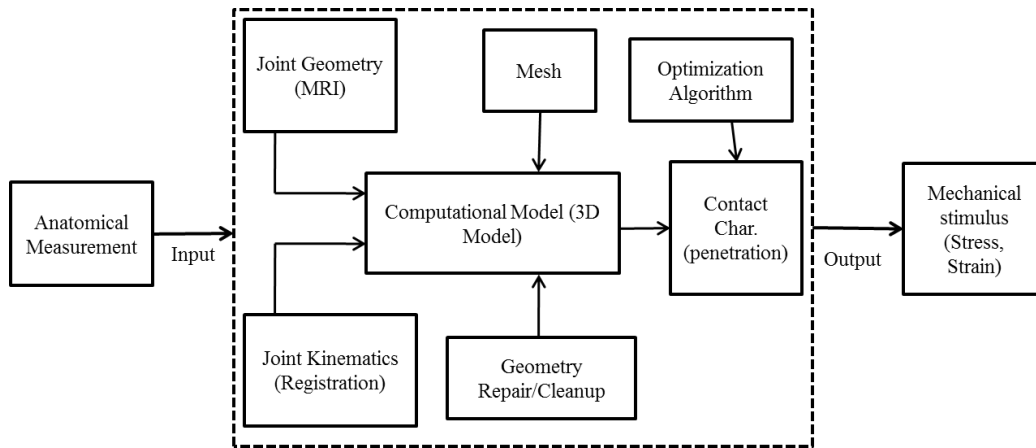


Figure 1: Computational model pipeline of PF joint

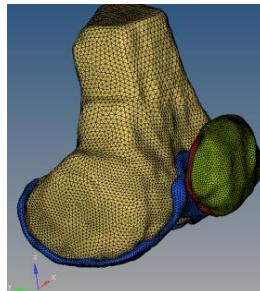


Figure 2: Finite element model of the PF joint (meshed model)

2.3 Statistical Analysis

Statistical analyses were performed using SPSS 17.0 (SPSS, Inc., Chicago, IL, USA). A one-tailed t-test was conducted, and significance was set at $p < 0.05$ to compare the penetration depth between healthy and PFPS subjects. Besides the t-test, a non-parametric statistical test called Wilcoxon signed-rank test was performed to verify the results obtained from t-test as the sample sizes were small. The Wilcoxon signed-rank test assumed that the samples were distribution free. A significance level of 0.1 was used to compare the difference in penetration depth between healthy and PFPS subjects.

3. Results

3.1 Alternative Geometric Methods

The PD of healthy and PFPS subjects for the left knee and the right knee are shown in Tables 2 and 3, respectively. The methods used to measure the PD have rendered different results.

Table 2: PD for left knee of Healthy and PFPS subjects at different knee positions

Knee Angle Position	Healthy Subject	PD ₁ $\sqrt[3]{mm^3}$	PD ₂ (mm)	PD ₃ $\left(\frac{mm^3}{mm^2}\right)$	PD ₄ $\left(\frac{mm}{mm}\right)$	PD ₅ (mm)
30°	1	6.08	1.95	1.10	0.97	2.20
	2	6.97	1.98	1.54	1.95	2.80
	3	6.50	1.90	1.16	1.81	2.40
45°	1	6.88	2.20	1.10	1.41	2.60
	2	7.50	2.10	1.24	2.43	3.00
	3	7.32	1.98	1.10	2.58	2.50
Knee Angle Position	PFPS	PD ₁ $\sqrt[3]{mm^3}$	PD ₂ (mm)	PD ₃ $\left(\frac{mm^3}{mm^2}\right)$	PD ₄ $\left(\frac{mm}{mm}\right)$	PD ₅ (mm)
30°	1	7.13	3.18	1.33	2.27	2.95
	2	6.93	3.00	1.52	1.46	2.90
	3	5.30	2.00	0.67	1.04	1.90
45°	1	7.59	3.36	1.36	2.75	3.10
	2	8.25	3.38	1.39	2.50	2.92
	3	7.68	2.20	1.36	3.10	2.90

Table 3: PD for right knee of Healthy and PFPS subjects at different knee positions

Knee Angle Position	Healthy Subject	PD ₁	PD ₂	PD ₃	PD ₄	PD ₅
		$\sqrt[3]{mm^3}$	(mm)	$\left(\frac{mm^3}{mm^2}\right)$	$\left(\frac{mm}{mm}\right)$	(mm)
30°	1	3.46	1.3	0.53	0.27	1.1
	2	5.36	1.6	0.74	0.887	1.8
	3	4.098	1.29	0.58	0.48	1.3
45°	1	5.274	1.6	0.93	0.96	1.9
	2	5.9	1.97	0.78	1.2	2.15
	3	4.313	1.47	0.46	0.56	1.35
Knee Angle Position	PFPS	PD ₁	PD ₂	PD ₃	PD ₄	PD ₅
		$\sqrt[3]{mm^3}$	(mm)	$\left(\frac{mm^3}{mm^2}\right)$	$\left(\frac{mm}{mm}\right)$	(mm)
30°	1	4.44	1.8	0.47	0.62	1.72
	2	4.14	1.47	0.37	0.5	1.35
	3	4.54	1.2	0.45	0.62	1.15
45°	1	7.83	3.6	1.284	3.41	3.55
	2	6.73	3.61	1.1	2.05	3.53
	3	6.31	2.38	0.83	1.7	2.3

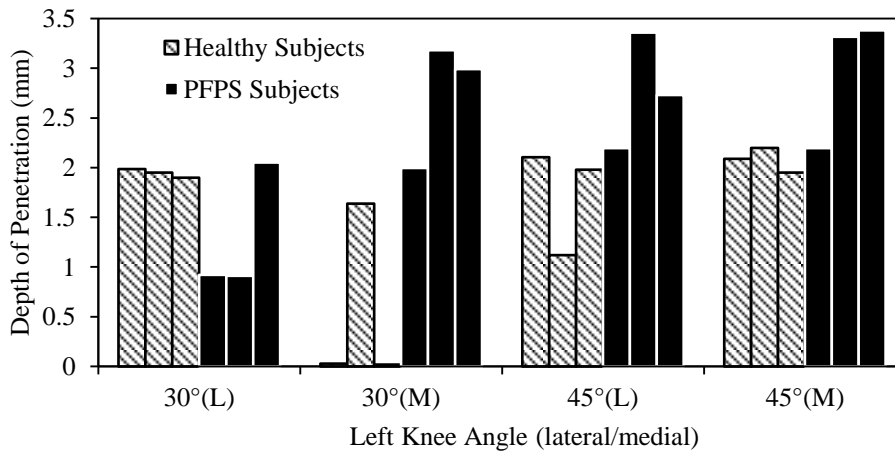


Figure 3: PD (mm) in lateral (L) and medial (M) side of the PF joint for healthy and PFPS subjects at the 30° and 45° left knee positions using method PD₂

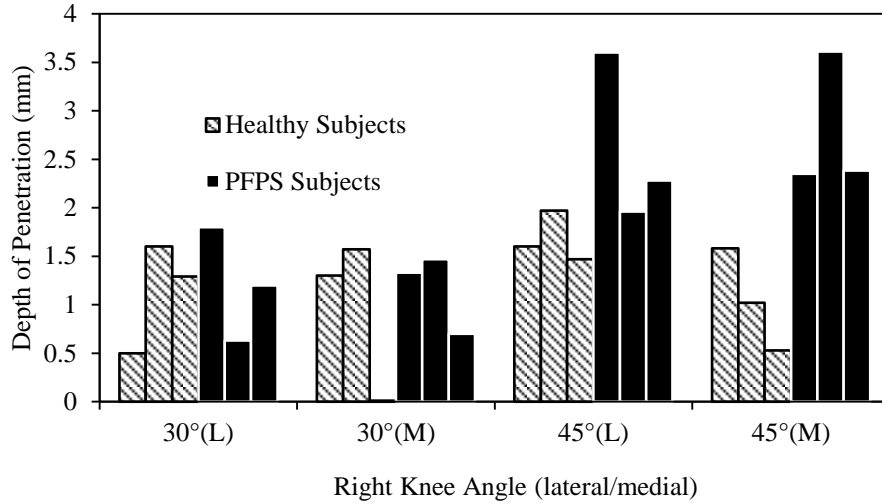


Figure 4: PD (mm) in lateral (L) and medial (M) side of the PF joint for healthy and PFPS subjects at the 30° and 45° right knee positions using method PD₂

Figure 3 and 4 depict the variation in the PD between the lateral and medial sides of the PF joints for both healthy and PFPS subjects using method PD₂. All methods (i.e., PD₁- PD₅) provided distinction between healthy and PFPS subjects at 30° and 45° knee positions. However, only method PD₂ was able to distinguish between medial and lateral compartment of the PF joint, so it was selected for further analysis.

In both healthy and PFPS subjects for both left and right knees, PD₁, PD₂, PD₄, and PD₅ show that the PD increases as the knee flexion angle increases. PD₃ has an opposite trend for left and right knees of healthy subjects, as well as for the left knee of PFPS subjects. PD is greater for PFPS subjects at 30° for both left and right knees, but results of the t-tests and Wilcoxon signed-rank test suggest that differences between healthy and PFPS subjects at a 30° knee flexion angle were not statistically significant. A significant difference was found between healthy and PFPS subjects ($p < 0.05$) for the left knee using PD₁ and PD₃ at 45° knee flexion angle. In the case of the right knee, PFPS subjects have significantly higher PD ($p < 0.05$) compared to the healthy subjects using all methods (i.e., PD₁-PD₅). Similar results were found using the Wilcoxon signed-rank test, but it

showed significant difference between healthy and PFPS subjects ($p=0.109$) at the 30° right knee flexion angle using PD_3 , as well as a significant difference between healthy and PFPS subjects ($p=0.109$) at the 30° left knee flexion angle using PD_2 .

Table 4: Statistical Analysis results (p-values from t-test)

Knee Angle Position (left knee)	PD_1	PD_2	PD_3	PD_4	PD_5
30° Healthy and PFPS	0.465	0.076	0.350	0.492	0.388
45° Healthy and PFPS	0.019	0.059	0.013	0.11	0.133
Knee Angle Position (right knee)	PD_1	PD_2	PD_3	PD_4	PD_5
30° Healthy and PFPS	0.464	0.346	0.092	0.445	0.492
45° Healthy and PFPS	0.035	0.020	0.0008	0.047	0.011

Table 5: Statistical Analyses results (p-values from Wilcoxon signed-rank test)

Knee Angle Position (left knee)	PD ₁	PD ₂	PD ₃	PD ₄	PD ₅
30° Healthy and PFPS	0.593	0.109	0.593	1.0	0.593
45° Healthy and PFPS	0.109	0.109	0.102	0.109	0.285

Knee Angle Position (right knee)	PD ₁	PD ₂	PD ₃	PD ₄	PD ₅
30° Healthy and PFPS	1.0	1.0	0.109	1.0	1.0
45° Healthy and PFPS	0.109	0.109	0.109	0.109	0.109

Table 6: Statistical Analysis results for medial and lateral side of PF joint (right knee)

Penetration depth p-value for Right Knee			
30° Healthy and PFPS		45° Healthy and PFPS	
Lat	Med	Lat	Med
0.457	0.24	0.124	0.04

Table 7: Statistical Analysis results for medial and lateral side of PF joint (left knee)

Penetration depth p-value for Left Knee			
30° Healthy and PFPS		45° Healthy and PFPS	
Lat	Med	Lat	Med
0.105	0.018	0.119	0.056

A higher PD occurred on the medial side of the PFPS joint at a 30° flexion, and it was statistically significant (p=0.018) for the left knee. For the 45° knee flexion

angle, a slight increase of PD was obtained, and it was statistically significant ($p=0.04$) for the right knee.

3.2 Simulation results of Finite Element Modeling

The contact pressure and von Mises stress in cartilage were shown to increase with flexion in both healthy and PFPS joints, and the largest values were obtained in the PFPS joint (Fig. 6). Higher contact pressure occurred on the medial side of the PFPS joint and shifted to the lateral side for the healthy joint (Fig. 6). A similar trend was obtained for von Mises stress (Fig.7). Figure 5 depicts the von Mises stress distribution in the patellar cartilage surface for healthy as well as symptomatic PF joint at 30° and 45° knee flexion angle conditions.

Table 8: Peak von Mises stresses (MPa) for Healthy and PFPS subjects at patellar cartilage surface

Knee Angle Position	Subject	Contact Pressure	Von Mises Stress	Max. Principal Stress
30°	Healthy	3.84	2.10	4.61
45°		6.23	5.80	6.98
30°	PFPS	5.37	2.55	7.05
45°		5.76	6.55	12.18

Table 9: Peak von Mises stresses (MPa) for Healthy and PFPS subjects at femoral cartilage surface

Knee Angle Position	Subject	Contact Pressure	Von Mises Stress	Max. Principal Stress
30°	Healthy	3.77	1.81	4.47
45°		4.71	3.24	6.98
30°	PFPS	4.32	2.66	6.08
45°		6.73	3.63	5.60

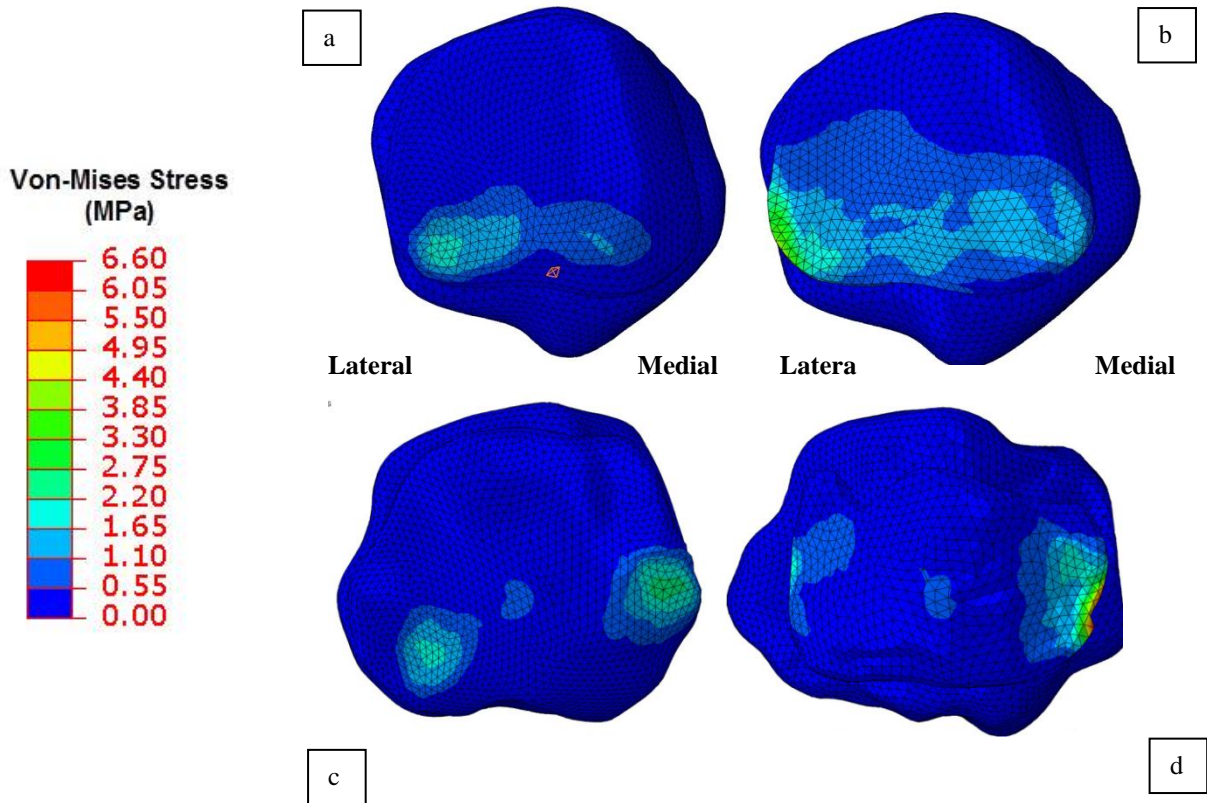


Figure 5: Patellar cartilage von Mises stress distribution for cases (a) Healthy knee at 30° (max. stress of 2.1 MPa at lateral side), (b) Healthy knee at 45° (max. stress of 5.80 MPa at lateral side), c) PFPS knee at 30° (max. stress of 2.55 MPa at medial side), and d) PFPS knee at 45° (max. stress of 6.55 MPa at medial side).

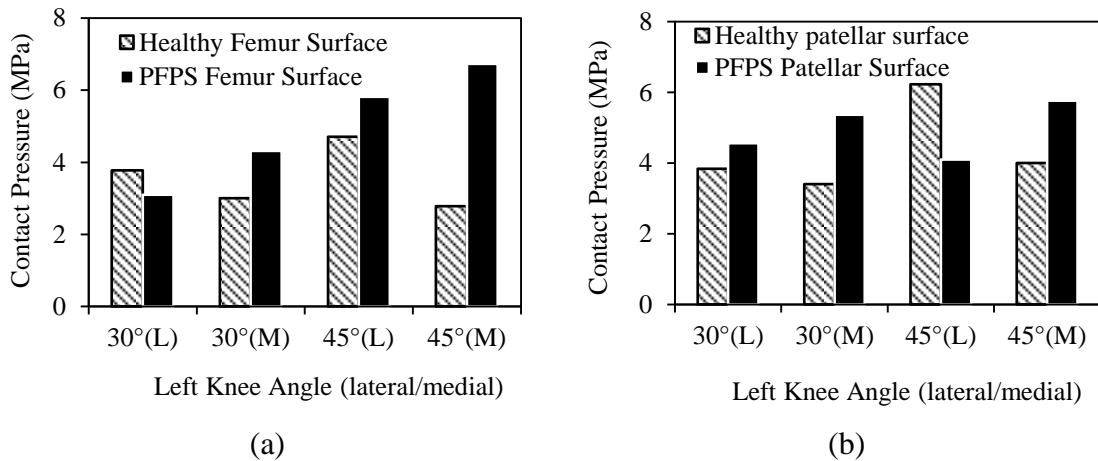


Figure 6: Contact pressure in lateral (L) and medial (M) side of the PF joint at 30° and 45° flexion for healthy and PFPS joints at: (a) femur cartilage surface and (b) patellar cartilage surface

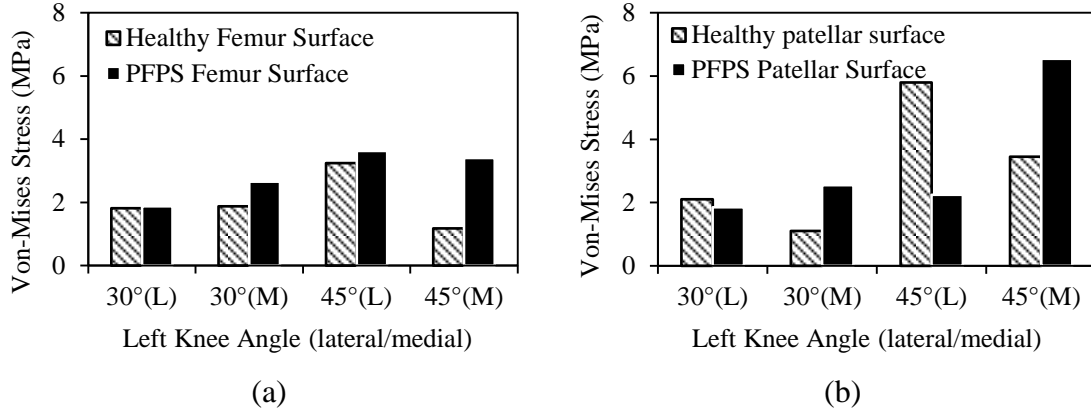


Figure 7: Maximum von Mises stresses (MPa) in lateral (L) and medial (M) side of the PF joint (femur cartilage (Fig. 5a) and patellar cartilage (Fig. 5b) for healthy and PFPS subjects at different knee positions.

4. Discussions

The purpose of this study has been to quantify the contact stresses in the PF joints for healthy and symptomatic joints. To fulfill this purpose, the FEA of the PF joints for healthy and pathological subjects at two different knee flexion angles have been investigated. In addition to the FEA, another geometric approach has been developed to investigate the joint contact behaviour for both healthy and PFPS subjects. FEA is used to generate stress maps where stresses are generally quantified based on the gradients of the deformation of the model. In the alternate geometric method, the same 3D geometry have been utilized that are used in FEA, in order to identify the location of high gradients of deformation without the cumbersome task of generating FEA models where material property, FE meshing of the complex 3D geometry, muscle forces, joint lubrications, appropriate boundary conditions, and contact stresses which are subjected to user discretion must be dealt with.

From the current study we have demonstrated that the contact deformation is related to the virtual penetration depth (PD) of the joint's femoral and patellar cartilage surfaces, measured using the 3D registration and linear mapping of the patella from 15° (reference position) to 30° and 45° knee flexion angles. Five different measurement techniques were used to measure PD in six healthy and six

PFPS female knee joints.

Contact areas between the femur and patellar cartilage surfaces are extended from the medial to the lateral side of the PF joints (Clark et al. 2002). Therefore, the location of the maximum contact stress could be in the lateral, central, or medial side of the contact surface. In the present study, the location of the peak contact stress was found in the lateral side of the patellar cartilage surface for a healthy subject using finite element models, which is consistent with those reported in the literature for healthy subjects (Besier et al. 2005; Farrokhi et al. 2011). In addition, we found that the PD was also greatest on the lateral side for 5 of the 6 healthy knees at 30° and 45° knee flexion angles. One healthy subject showed a higher PD on the medial side at 30°, and another healthy subject showed a higher PD on the medial side at a 45° knee flexion angle. Contact stresses and von Mises stresses increased with knee flexion from 30° to 45°. Penetration depth also increased with knee flexion from 30° to 45°.

Contact stresses reported in the literature for PFPS subjects are controversial and generally higher in the lateral side of the PF joints (Farrokhi et al. 2011). However, the present study has shown PFPS subjects to have a higher PD on the medial side compared to healthy subjects, and the values were statistically significant. The current FEA showed higher stresses in the medial side of the PFPS subject which is consistent with the results obtained from the alternative geometric method. One recent study has found increased bone metabolic activity in the posterior side of the patella (Draper et al. 2012), as well as increased bone metabolic activity on both the medial and lateral sides of the patella for subjects with chronic knee pain (Draper et al. 2012).

It has been reported that due to the muscle imbalance, the patella shifts and tilts laterally, causing an overloading in the lateral facet (Ahmed et al. 1983; Cowan et al. 2009; Dhaher and Kahn 2002; Lee et al. 2002; Wilson et al. 2009). Our study confirmed the lateral shift of the contact area using the alternate geometric method

and FEA. On the other hand, peak stresses and PD location were observed in the medial side for PFPS subjects, in contradiction to most of the current literature. However, Sawatsky et al. (2012) have shown that the muscle imbalance associated with PFPS did not cause shifting in the contact pressure. Furthermore, a recent study by Draper et al. (2012) has found an increased bone metabolic activity on the medial side for a few subjects, Gorniak (2009) found greater cartilage wear on the medial side compared to the lateral side of PF joints of the cadaveric specimen, and Song et al. (2011) also reported in their review article that symptomatic patella did not consistently show lateral malalignment or maltracking. These findings support our results, demonstrating that higher stresses occur in the medial side of the PF joint in PFPS subjects. PD estimation using the alternate geometric method reveals similar trends to those in the FEA results.

Other previous studies have found octahedral shear stress to be higher in the patellar cartilage surface compared to the femur cartilage surface (Besier et al. 2005; Farrokhi et al. 2011), and higher bone metabolic activity in the patella compared to the femur (Draper et al. 2012). In the present study we also found higher stresses in the patellar cartilage surface in both healthy and PFPS subjects.

PD estimated using various methods (PD_1 to PD_5) is greater in PFPS subjects. Finite element models also show higher stresses in the PFPS subjects, a result which corresponds to the quantification of the PD using alternate geometric method. In both FEA and the alternate geometric method, the present study found that the PFPS subjects experienced higher stresses compared to the healthy subjects, which is consistent with the current literature (Farrokhi et al. 2011). Our results reveal that contact stress is related to penetration depth. FEA and the alternate geometric method show similar trends in both the healthy and PFPS subjects. Moreover, the alternate geometric method could be a robust useful tool to assess PFPS.

This study has shown, using both FEA and alternative geometric method, that

PFPS subjects experience higher stress on the medial side of the PF joint compared to healthy subjects, which is contrary to the clinical idea that the greatest load occurs through the lateral facet, thereby causing higher stress in the lateral side and not the medial side. According to the earlier studies, as the PF joint reaction force is directed laterally, it will create higher pressure in the lateral facet (Hefzy and Yang 1993; Hirokawa 1991). In the current study we are focusing on the stress, not the force.

There are certain limitations in the present study. It is to be noted that all the subjects used in this study were tested in a supine condition during MRI, and the applied load was less than the body weight of the test subject. The results of this small sample size show general trends that were statistically confirmed with the t-test and Wilcoxon test, but additional subjects will be investigated in the future in order to further substantiate these findings.

5. Conclusions

The results presented in this paper should be considered as a “proof of concept”. The alternative geometric method proposed in this study is based on mathematical concepts. An accurate reconstruction of 3D models from MRI is an important issue in the present approach. Results of the present approach also depend on how accurately the patellar cartilage boundary and the femur cartilage boundary are identified. One clear distinction from the previous study was found in terms of the location of maximum stress for PFPS subjects. In previous studies, the lateral side of the PF joints was mentioned as critical for patellofemoral pain. The current study found the medial side of the PF joints for PFPS subjects to be significant. It should be noted that the current study is primarily focused on the magnitude and location of the maximum contact stress, as well as penetration depth. The results of the current study have shown that the medial side of the PF joint is also important in terms of PF pain, a finding which was not reported in the previous

studies. However, the proposed alternative geometric method to investigate the PFPS is computationally-efficient compared to the conventional FEA, and has the potential to effectively assess PFPS. Future work is required in order to evaluate the present approach on more subjects to establish it as a “gold standard” diagnostic/computational tool for patients with PFPS.

Conflict of interest statement:

The Authors have no conflict of interest to declare.

Acknowledgements:

We thank Amin Komeili and Behzad Vafaeian for their thoughtful ideas and comments throughout this work. This research work was partially supported by the Natural Sciences and Engineering Research Council (NSERC) of Canada.

References

- Adeeb, S. M. (2004). “Load-Bearing Across Diarthrodial Joints with special reference to peripheral structures and the menisci of the knee.” Ph.D Thesis, University of Calgary, Calgary.
- Ahmed, A. M., Burke, D. L., and Yu, A. (1983). “In-vitro measurement of static pressure distribution in synovial joints--Part II: Retropatellar surface.” *J Biomech Eng*, 105(3), 226–236.
- Besier, T. F., Gold, G. E., Beaupré, G. S., and Delp, S. L. (2005). “A modeling framework to estimate patellofemoral joint cartilage stress in vivo.” *Med Sci Sports Exerc*, 37(11), 1924–1930.
- Besier, T. F., Gold, G. E., Delp, S. L., Fredericson, M., and Beaupré, G. S. (2008). “The influence of femoral internal and external rotation on cartilage stresses within the patellofemoral joint.” *J. Orthop. Res.*, 26(12), 1627–1635.
- Biscević, M., Tomić, D., Starc, V., and Smrke, D. (2005). “Gender differences in knee kinematics and its possible consequences.” *Croat. Med. J.*, 46(2), 253–260.
- Clark, A. L., Herzog, W., and Leonard, T. R. (2002). “Contact area and pressure distribution in the feline patellofemoral joint under physiologically meaningful loading conditions.” *J Biomech*, 35(1), 53–60.
- Connolly, K. D. (2006). “In-vivo Characterization of Patellar Tracking in Normal

- and PFPS.” M. Sc. Thesis, University of Calgary, Calgary, AB, Canada.
- Cowan, S. M., Crossley, K. M., and Bennell, K. L. (2009). “Altered hip and trunk muscle function in individuals with patellofemoral pain.” *Br J Sports Med*, 43(8), 584–588.
- Csintalan, R. P., Schulz, M. M., Woo, J., McMahon, P. J., and Lee, T. Q. (2002). “Gender differences in patellofemoral joint biomechanics.” *Clin. Orthop. Relat. Res.*, (402), 260–269.
- Devereaux, M. D., and Lachmann, S. M. (1984). “Patello-femoral arthralgia in athletes attending a Sports Injury Clinic.” *Br J Sports Med*, 18(1), 18–21.
- Dhaher, Y. Y., and Kahn, L. E. (2002). “The effect of vastus medialis forces on patello-femoral contact: a model-based study.” *J Biomech Eng*, 124(6), 758–767.
- Draper, C. E., Fredericson, M., Gold, G. E., Besier, T. F., Delp, S. L., Beaupre, G. S., and Quon, A. (2012). “Patients with patellofemoral pain exhibit elevated bone metabolic activity at the patellofemoral joint.” *J. Orthop. Res.*, 30(2), 209–213.
- Elias, J. J., Wilson, D. R., Adamson, R., and Cosgarea, A. J. (2004). “Evaluation of a computational model used to predict the patellofemoral contact pressure distribution.” *Journal of Biomechanics*, 37(3), 295–302.
- Fairbank, J. C., Pynsent, P. B., van Poortvliet, J. A., and Phillips, H. (1984). “Mechanical factors in the incidence of knee pain in adolescents and young adults.” *J Bone Joint Surg Br*, 66(5), 685–693.
- Farrokhi, S., Keyak, J. H., and Powers, C. M. (2011). “Individuals with patellofemoral pain exhibit greater patellofemoral joint stress: a finite element analysis study.” *Osteoarthr. Cartil.*, 19(3), 287–294.
- Fisher, S., and Lin, M. C. (2001). “Fast penetration depth estimation for elastic bodies using deformed distance fields.” *Intelligent Robots and Systems, 2001. Proceedings. 2001 IEEE/RSJ International Conference on*, 330–336.
- Fulkerson, J. P. (2002a). “Diagnosis and Treatment of Patients with Patellofemoral Pain.” *Am J Sports Med*, 30(3), 447–456.
- Fulkerson, J. P. (2002b). “Diagnosis and Treatment of Patients with Patellofemoral Pain.” *Am J Sports Med*, 30(3), 447–456.
- Gorniak, G. C. (2009). “Patterns of patellofemoral articular cartilage wear in cadavers.” *J Orthop Sports Phys Ther*, 39(9), 675–683.
- Han, S. K., Federico, S., Epstein, M., and Herzog, W. (2005). “An articular cartilage contact model based on real surface geometry.” *Journal of biomechanics*, 38(1), 179–184.
- Hefzy, M. S., and Yang, H. (1993). “A three-dimensional anatomical model of the human patello-femoral joint, for the determination of patello-femoral motions and contact characteristics.” *Journal of Biomedical Engineering*, 15(4), 289–302.
- Hirokawa, S. (1991). “Three-dimensional mathematical model analysis of the patellofemoral joint.” *Journal of biomechanics*, 24(8), 659–671.
- Huberti, H. H., Hayes, W. C., and others. (1984). “Patellofemoral contact pressures. The influence of q-angle and tendofemoral contact.” *The*

- Journal of bone and joint surgery. American volume*, 66(5), 715.
- Lee, T. Q., Morris, G., and Csintalan, R. P. (2003). "The influence of tibial and femoral rotation on patellofemoral contact area and pressure." *J Orthop Sports Phys Ther*, 33(11), 686–693.
- Lee, T. Q., Sandusky, M. D., Adeli, A., McMahan, P. J., and others. (2002). "Effects of simulated vastus medialis strength variation on patellofemoral joint biomechanics in human cadaver knees." *Journal of rehabilitation research and development*, 39(3), 429–438.
- Loud, K. J., and Micheli, L. J. (2001). "Common athletic injuries in adolescent girls." *Curr. Opin. Pediatr.*, 13(4), 317–322.
- Mach, D. B., Rogers, S. D., Sabino, M. C., Luger, N. M., Schwei, M. J., Pomonis, J. D., Keyser, C. P., Clohisy, D. R., Adams, D. J., O'Leary, P., and Mantyh, P. W. (2002). "Origins of skeletal pain: sensory and sympathetic innervation of the mouse femur." *Neuroscience*, 113(1), 155–166.
- Malinzak, R. A., Colby, S. M., Kirkendall, D. T., Yu, B., and Garrett, W. E. (2001). "A comparison of knee joint motion patterns between men and women in selected athletic tasks." *Clin Biomech (Bristol, Avon)*, 16(5), 438–445.
- Mesfar, W., and Shirazi-Adl, A. (2005). "Biomechanics of the knee joint in flexion under various quadriceps forces." *The Knee*, 12(6), 424–434.
- Neptune, R. R., Wright, I. C., and van den Bogert, A. J. (2000). "The influence of orthotic devices and vastus medialis strength and timing on patellofemoral loads during running." *Clin Biomech (Bristol, Avon)*, 15(8), 611–618.
- Ong, C.-J. (1997). "On the Quantification of Penetration between General Objects." *The International Journal of Robotics Research*, 16(3), 400–409.
- Powers, C. M. (2003). "The influence of altered lower-extremity kinematics on patellofemoral joint dysfunction: a theoretical perspective." *J Orthop Sports Phys Ther*, 33(11), 639–646.
- Powers, C. M., Landel, R., and Perry, J. (1996). "Timing and intensity of vastus muscle activity during functional activities in subjects with and without patellofemoral pain." *Physical Therapy*, 76(9), 946–955.
- Ronsky, J. L., Herzog, W., Brown, T. D., Pedersen, D. R., Grood, E. S., and Butler, D. L. (1995). "In vivo quantification of the cat patellofemoral joint contact stresses and areas." *J Biomech*, 28(8), 977–983.
- Sawatsky, A., Bourne, D., Horisberger, M., Jinha, A., and Herzog, W. (2012). "Changes in patellofemoral joint contact pressures caused by vastus medialis muscle weakness." *Clin Biomech (Bristol, Avon)*, 27(6), 595–601.
- Sheehan, F. T., Borotikar, B. S., Behnam, A. J., and Alter, K. E. (2012). "Alterations in in vivo knee joint kinematics following a femoral nerve branch block of the vastus medialis: Implications for patellofemoral pain syndrome." *Clin Biomech (Bristol, Avon)*, 27(6), 525–531.
- Sheehan, F. T., Derasari, A., Brindle, T. J., and Alter, K. E. (2009). "Understanding patellofemoral pain with maltracking in the presence of joint laxity: Complete 3D in vivo patellofemoral and tibiofemoral

- kinematics.” *Journal of Orthopaedic Research*, 27(5), 561–570.
- Song, C.-Y., Lin, J.-J., Jan, M.-H., and Lin, Y.-F. (2011). “The role of patellar alignment and tracking in vivo: the potential mechanism of patellofemoral pain syndrome.” *Phys Ther Sport*, 12(3), 140–147.
- Stammberger, T., Hohe, J., Englmeier, K. H., Reiser, M., and Eckstein, F. (2000). “Elastic registration of 3D cartilage surfaces from MR image data for detecting local changes in cartilage thickness.” *Magn Reson Med*, 44(4), 592–601.
- Tang, M., Lee, M., and Kim, Y. J. (2009). “Interactive Hausdorff distance computation for general polygonal models.” *ACM Trans. Graph.*, 28(3), 74:1–74:9.
- Wilson, N. A., Press, J. M., Koh, J. L., Hendrix, R. W., and Zhang, L. Q. (2009). “In vivo noninvasive evaluation of abnormal patellar tracking during squatting in patients with patellofemoral pain.” *The Journal of Bone and Joint Surgery. American volume.*, 91(3), 558.
- Zhang, L., Kim, Y. J., Varadhan, G., and Manocha, D. (2007). “Generalized penetration depth computation.” *Computer-Aided Design*, 39(8), 625–638.

Chapter 3: Three-Dimensional Geometric Analysis of the Talus for designing Talar Prosthetics

A Journal Paper will be submitted to the Journal of Biomechanics:

This paper is presented in the next chapter with the title: “**Paper II**”

Paper II
**Three-Dimensional Geometric Analysis of the Talus for designing Talar
Prosthetics**

Kamrul Islam^a, Kajsa Duke^b, Walied Hajar^a, Ashlee Dobbe^c, Marwan El-rich^a,
Nadr Jomha^c and Samer Adeeb^a

*^aDepartment of Civil and Environmental Engineering, University of Alberta,
Canada; ^bDepartment of Mechanical Engineering, University of Alberta, Canada;
^cFaculty of Medicine and Dentistry-Division of Orthopaedic Surgery, University
of Alberta, Canada*

Corresponding Author:

Kamrul Islam
Department of Civil and Environmental Engineering
Markin/CNRL Natural Resources Engineering Facility
9105 116th St
Edmonton, Alberta, Canada
T6G 2W2

Phone: 1(780) 492 3718

Email: kamrul1@ualberta.ca

Abstract:

Proper understanding of the complex geometric shape of the talus bone is very important for the design of custom made talar body prosthetics and the restoration of the proper ankle joint function after surgery. To date, all of the talus implants are patient-specific with the limitation that the shape does not resemble the proper geometric shape of the talus. Therefore, it is important to perform a thorough investigation of the geometric shape of the talus bone. This paper addresses the applicability of a scaling approach for investigating the geometric shape and similarity of the talus bones. Furthermore, five different sizes of talus implants are proposed. This study uses CT scan images of the ankle joints of 27 different subjects to perform the analysis. Results of the deviation analyses show the deviation in the articulating surfaces of the talus bones are not excessive in terms of talus size. This has revealed that the proposed five implant sizes are promising, as well as they could resolve the long standing problem of the ankle bone replacement surgery by restoring proper joint kinematics. Finally, it is concluded that the talus bones of the ankle joints are geometrically similar and the proposed implant sizes fit a wide range of subjects which could help to develop generic talus implants that might be applicable to all patients associated with talus injury.

Keywords: talus, geometric similarity, scaling, implants, deviation analysis

1. Introduction

The talus bone (Figure 1) is one of the most important and the second largest tarsal bone in the foot. With the majority of its surface covered with a thin layer of articular cartilage, it transmits the entire load of the lower portion of the musculo-skeletal system (Salathé, Arangio, and Salathé 1986; A Leardini 2001; Manter 1946; Sugimoto et al. 2005; Akiyama et al. 2012). It has no muscle attachments, and the vascular supply of the talus bone is maintained by the ligaments, synovial tissue, and joint capsules (Fortin and Balazsy 2001). Major injuries to the talus bone are infrequent; however talar fractures are second in frequency to all tarsal bone fractures (Fortin and Balazsy 2001; Kenwright and Taylor 1970; Berlet, Lee, and Massa 2001; Huang and Cheng 2005). In fact, the occurrence of the talar fractures account for only 0.1 to 0.85% of all skeletal fractures (Santavirta et al. 1984). Among all ankle-foot injuries, around 3% are related to talar fractures where approximately 50% of these fractures are reported in the talar neck (Lesic and Bumbasirevic 2004; Daniels and Smith 1993; Inokuchi, Ogawa, and Usami 1996). Additionally, patients with ankle osteoarthritis, which amount to 6-13% of all cases of osteoarthritis, can develop debilitating conditions that can be more severe than hip arthritis (Glazebrook et al. 2008).

The integrity of the talus is essential to normal function of the ankle, subtalar and transverse tarsal joints. As a result of both the function of the talus and its fragile blood supply, talus fractures can result in permanent pain, loss of motion, and deformity (Fortin and Balazsy 2001). Fracturing of the talus bone is a common occurrence in younger members of the population that can result in death of the bone with subsequent collapse and development of severe osteoarthritis. Given these realities, talus bone replacement through the use of an implant has become a well needed option in orthopaedic surgery in order to promote proper functioning of the ankle joint (Glazebrook et al. 2008; Alberto Leardini 2001; Conti and Wong 2001; Seth 2011).

The restoration of proper ankle joint function through surgery is an unresolved challenge due to the lack of refinement of implant design for whole talar replacements. Proper joint kinematics not only depends on the load-carrying capacities of the implants, but also on restoring the proper three dimensional shape (i.e., complex articulating surfaces). Therefore, better understandings of ankle anatomy and morphology are integral to successful talus bone replacement using an implant.

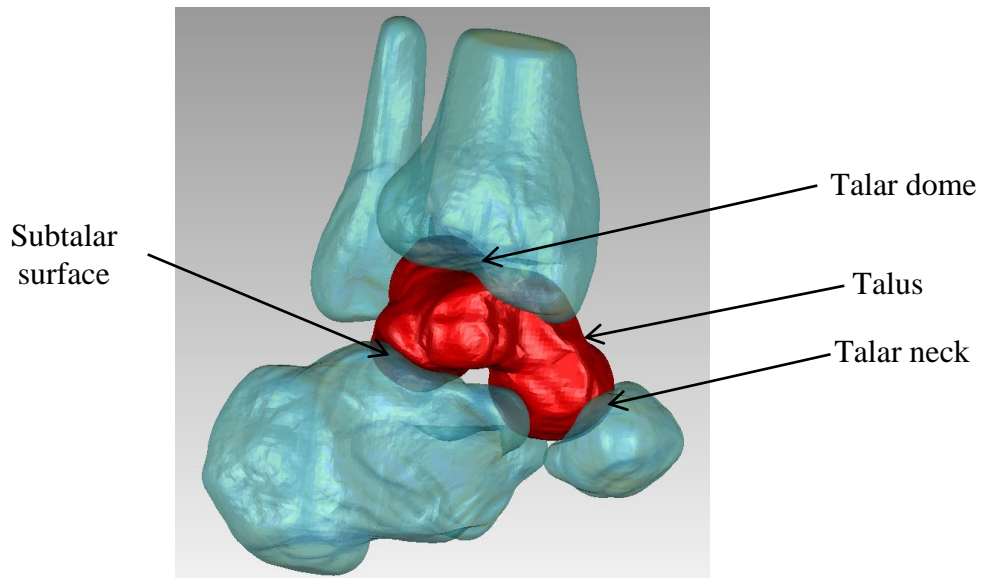


Figure 1: 3D geometry of ankle-foot complex

The anatomy and geometry of the ankle joint are complex in nature. Attempts were made by biomechanic researchers to describe the anatomy and geometry of the ankle joint using various techniques. However, the complete three dimensional morphology of the ankle joint is still unclear. Early geometric studies of the talus bone relied on 2D radiographic data to obtain the correlation between various two dimensional distances using direct measurement (Fessy, Carret, and Béjui 1997) and automatic measurement techniques (Stagni et al. 2004; Stagni et al. 2005). However, 2D measurements did not capture the complex nature of the geometry of the talus bone. Although, high resolution 3D computed tomography (CT) images were used to mimic the in-vivo bone morphology in the past (Andrea

Hayes, YukiTochigi, and Charles 2012; van Schaik, Verbiest, and van Schaik 1985; Müller et al. 1996), yet, very few studies were done to date on the topographic analyses of talus bone of the ankle joint. Recently, high resolution 3D computed tomography (CT) images were used to show that there is a significant gender dependent variation in the dimensions of the talus among the population (Andrea Hayes, YukiTochigi, and Charles 2012). However, in the case of CT images, the researchers did not correlate the various measured dimensions with the actual size of the talus bone which is readily available within the collected data.

Based on the ankle morphology, various studies have developed ankle prosthesis over time for the better replacement of the damaged ankle-foot complex to retain the functionality of the joint. Recently, Kakkar and Siddique (2011), Barton et al. (2011), and Seth (2011) conducted excellent literature reviews on the total ankle replacement (TAR) using prosthesis, and addressed the associated biomechanical changes after implantation. Those studies gave a clear in-sight about the previous research works on TAR.

Numerous studies have also reported the incorporation of the custom made talar body implant in the patients with severely damaged talus (Harnroongroj and Vanadurongwan 1997; Tanaka et al. 2003; Magnan, Facci, and Bartolozzi 2004; Stevens et al. 2007). The earliest attempt to replace the talus with an anatomically similar implant was reported in 1997. Stainless steel talar prostheses were manufactured based on the size and dimensions of the contralateral talus and placed in sixteen different patients who had experienced fracture or bone necrosis of the talus bone (Harnroongroj and Vanadurongwan 1997). A similar procedure was reported utilizing alumina ceramic talus prosthesis in 2003. Tanaka et al. (2003) replaced collapsed talar bodies in three patients with a prosthesis that was cemented to part of the talus that was intact. Magnan et al. (2004) mentioned a case study where the talar prosthesis was designed based on the CT images utilizing the real bone geometry. Stevens et al. (2007) also used custom made

cobalt-chrome talar prosthesis for replacing the damaged talus bone. The prosthesis was designed based on the real talus geometric shape using the CT-scan images.

Therefore, talus bone replacement has received considerable attention in orthopaedic surgery in recent days. Proper replacement of the talus bone requires a thorough understanding of the complex geometric shape of the bone. The first objective of this present study is use a scaling approach to analyse the three dimensional talus geometry to investigate whether the talus bones are geometrically similar in shape. Another objective is to standardise the sizing of the talus bone implants into five groups which will fit a wide range of talus injury patients.

The scaling approach is a common concept which has been used in the different engineering fields of application. Bazant (1984) proposed fracture mechanics based size-effect law where as Carpinteri and Chiaia (1997) proposed fractal based scaling laws. But all those scaling theories (Zdeněk P. Bažant 1984; Carpinteri and Chiaia 1997; Zdenek P. Bažant 2005) were related to the structural strength of materials. Carpenteri and Pugno (2005) described the scaling laws phenomena in geometric point of view. West and Brown (2004) showed the application of allometric scaling laws on biological systems. West et al. (1999) showed fractal analogy and it's correlation with allometric scaling. They also showed a comparison of scaling power of length, area and volume of the geometry in fractal analogy and conventional Euclidean perspective.

Various scaling models were proposed over time to describe the skeletal structures of various species. Among them the geometric similarity model (Hill 1950), the elastic similarity model (McMahon 1973), and the static stress similarity model (McMahon 1975) are very popular (Miller et al. 2008). But all these three models were correlated with body mass. Millar et al. (2008) showed the respective scaling exponent for those three models. More recently, Parr et al. (2011) performed extensive analyses on the articular surface of the talus of

hominoid primates to quantify the scaling properties within the talus. However, they did not find any generalized rule for the articular scaling which was contrary with the earlier prediction of isometric scaling (Parr, Chatterjee, and Soligo 2011).

In the current study, however, we did not adopt any of the previously described approaches of the scaling law. We used an uniform scaling approach to perform the analysis. An uniform scaling function is defined as

$\mathcal{T}(x): \mathbb{R}^3 \rightarrow \mathbb{R}^3$ such that $\forall x \in \mathbb{R}^3: \mathcal{T}(x) = \alpha \cdot x$ where $\alpha \in \mathbb{R}$ and α is the scaling factor.

2. Materials and Methods

2.1 Study participants

We obtained random sets of CT data of healthy talar bones of 28 subjects (24 males and 4 females) from the University of Alberta Hospital (Table 1). All the talar bone geometries were verified by an expert Radiologist of the University of Alberta Hospital who has more than 15 years experiences whether the talus bones were intact or not. Ethics approval was obtained from University of Alberta Hospital to use the CT scans for analysis. All the subjects used in this study were scanned in a supine condition.

Table 1: Characteristics of the subjects

	Intact talus bone (n=28)		
	Mean	SD	Range
Age (years)	27	6	21-42

n= Number of subjects used in the study

2.2 Data format

Each CT scan data set was made up of an average 191 slices, and 512×512 pixels per slice. The pixel size of the CT scans is 0.36 mm with a constant slice thickness of 1mm.

2.3 Geometry construction

The CT scan machine software produced DICOM images which were then imported into the 3D image processing software, MIMICS (Materialize NV, Belgium). MIMICS is an image processing software which generates a 3D model using the segmented images of each CT slice. Pixel threshold values of 226 HU to 1810 HU were used for all subjects during the segmentation. However every slice of the CT scans was manually inspected and image artifacts were removed for better digitization of the talus bone geometry. Finally, 3D reconstructed geometry of the talus was created using MIMICS. During digitization of the images, it was found that one of the twenty-eight subjects had a minor posterior surface fracture. Therefore, to keep consistency (the other 27 subjects were intact) the results of this subject's talus bone was not included. Furthermore, in order to capture the inter-observer variability in digitizing the talus bone geometry, two independent observers created the geometry of the talus bone from four randomly picked subjects.

2.4 Data analysis

2.4.1 Geometric similarity and scaling of talus bone

Following the digitization; the 3D geometries of the talus bone were imported into the Geomagic Studio/Qualify 2012 (Raindrop Geomagic Inc.) as Stereolithography (STL) files. The STL files of all subjects were further modified using the built-in

mesh doctor feature to clean up the geometry in order to remove protruding vertices and localized holes in the 3D talus geometries.

In this study, in order to establish the applicability of the scaling approach, Subject Id 28 was set as the reference model (since it was the talus closest to the calculated average volume), and the other twenty-six subjects were used as target models. After quantifying the volume of all twenty seven subjects, the ratios of volume of the reference model (subject Id 28) to target models (subject Id 1, subject Id 2, subject Id 3,....., subject Id 27) were calculated, and finally the cubic roots of all twenty seven ratios ($\alpha_1, \alpha_2, \alpha_3, \dots, \alpha_{27}$) were estimated. Finally, the target models were scaled up by this number ($\alpha_1, \alpha_2, \alpha_3, \dots, \alpha_{27}$) using the custom uniform scaling tool bar of Geomagic Qualify. Afterwards, the reference model and target models (one at a time) were firstly positioned and roughly aligned using the built in algorithm “manual registration”. Again they (reference and target models) were aligned using another built in algorithm “best fit alignment” of Geomagic. Following the alignment, the two geometries were compared using a custom tool 3D comparison in order to quantify the 3D deviation. The 3D deviation analysis provides the deviation of the target model with respect to the reference model. The output parameters generated from the 3D comparisons showed a positive as well as a negative deviation (orthogonal distance) indicating that the surface of the target models is above or below the surface of the reference models respectively. The geometric similarity of the talus bones were verified by comparing the test models with the reference model using the 3D deviation analyses. Figure 2 depicts the chronological sequences to illustrate the methodology adopted in this section.

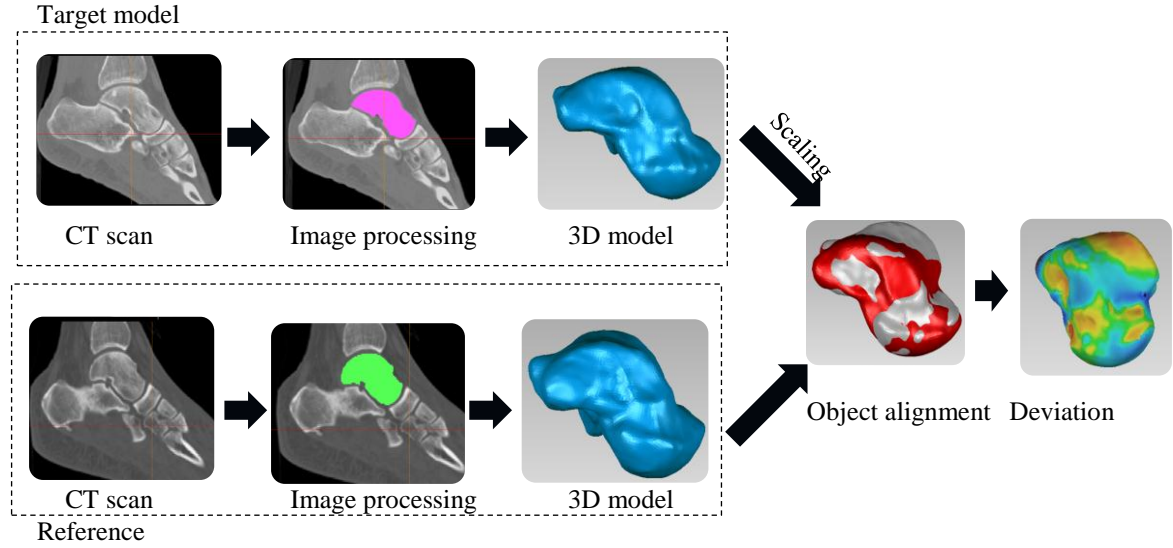


Figure 2: Flow diagram to illustrate the methodology

2.4.2 Template creation and different implant sizes

We calculated the average volume (V_{avg}) and the standard deviation (δ) of the twenty seven talus models. The talus model whose volume was close to the average value was chosen as the template model for implant creation. The template model was used to create five different sizes talus implants. The implants sizes were based on the addition and subtraction of the standard deviation (S.D) to the average volume ($V_{avg} - 2\delta$, $V_{avg} - \delta$, V_{avg} , $V_{avg} + \delta$, $V_{avg} + 2\delta$). Table 2 shows the volumes of the 5 different implant sizes.

Table 2: Implant Characteristics

Implant sizes	Volumes (mm ³)
Implant 1	26961.15
Implant 2	33810.44
Implant 3	40659.73
Implant 4	47509.02
Implant 5	54358.31

The implant models were generated using the similar scaling approach adopted in the previous section where template model was used as the reference model. After creating the implant models, all the twenty seven subjects were subdivided into five groups based on the volume nearest to the implant sizes. Figure 3 and 4 showed the distribution of the twenty seven subjects according to their corresponding implant sizes.

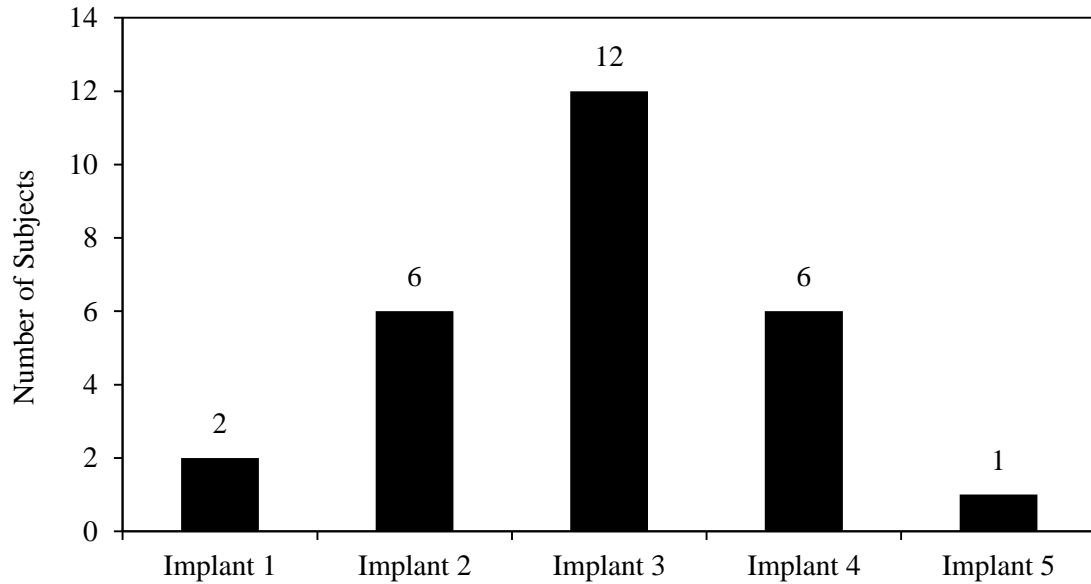


Figure 3: Distribution of the subjects

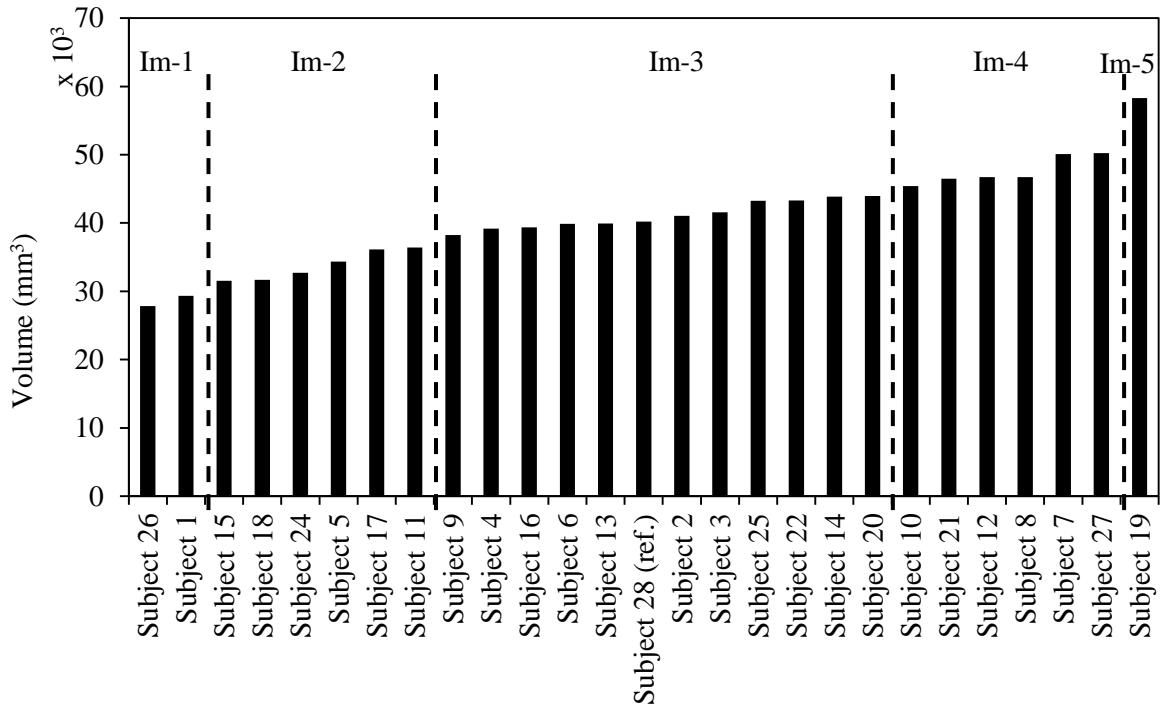


Figure 4: Volume of talus bones (Note: Im-1= Implant 1; Im-2= Implant 2 ; Im-3= Implant 3; Im-4= Implant 4; Im-5= Implant 5; ref.= reference)

The implant model size with the volume nearest to that of the subject's volume was used when comparing the implant to each subject. The selected implant size and specific subject were aligned using the procedure described in the previous section (using the manual registration and best fit alignment algorithm) for 3D comparison to quantify the deviation. It is to be noted that if the volume of the subject was almost middle of the two implants, in that case the subject was compared to the both implants, and whichever gave the smallest deviation was the one selected. Since the talus bone is very irregular in shape, we need to create the implant that will best fit a given patient's ankle joint. We are thus, in the interest of better design optimization, focusing the whole talus body as well as the three articulating surfaces i.e., talar dome (articulates with the tibial plafond), sub-talar surface (articulates with the calcaneus), and the talar neck (articulates with the navicular) of the talus bone. We quantified the average deviation in these three articulating surfaces as well.

3. Results

3.1 Inter-observer variability

Table 3: Inter-observer measurement (mm³)

Subjects	Observer 1 (volume)	Observer 2 (volume)	% difference
Subject Id 24	32994	32725	0.81
Subject Id 25	43729	43248	1.10
Subject Id 26	27509	27857	1.26
Subject Id 27	49139	50233	2.23

Table 3 shows the inter observer variation in digitizing the 3D geometries of the talus bones of the four subjects. Volume measurement was set as a base criterion in this study. It is also notable that the average inter-observer 3D deviation for the above four subjects was in the range of 0.03-0.26 mm.

3.2 Geometric similarity and scaling of talus bone

The volume of the talus bones of the reference model (subject Id 28) and target models are presented in Figure 4. Figure 5 depicts the 3D prototype models of the talus bone of four different subjects (from left: subject Id 26; subject Id 27; subject Id 25; subject Id 24) printed in a 3D printer using the VRML (virtual reality modelling language) file of Geomagic to better visualize the talus bones and see the complex shape and the three articulating surfaces.



Figure 5: 3D prototype models of 4 different talus bones.

Table 4 shows the detailed measurements and scaling factor (α) (described in the introduction) found using the scaling approach for 2 subjects. In this study we focused on the average deviation following the 3D comparison in order to mimic the global behavior of the scaling approach.

Table 4: Output of 3D model comparisons after incorporating the scaling approach (mm)

Target Model Id	Reference Model Volume (V_1)	Target Model Volume (V_2)	Scaling Factor, $\alpha = \sqrt[3]{\frac{V_1}{V_2}}$	Average Deviation Between Reference and New Target Model (+/-)
subject 1	40195	29323	1.111	+0.956/-0.916
subject 5	40195	34332	1.054	+0.572/-0.561

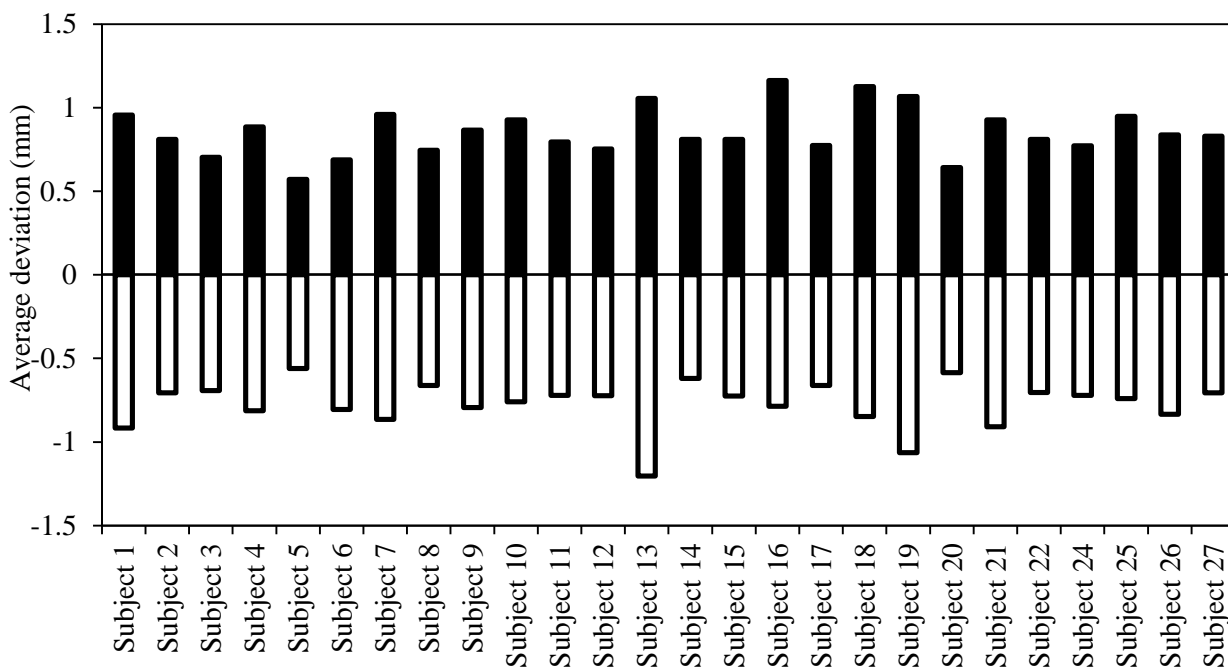


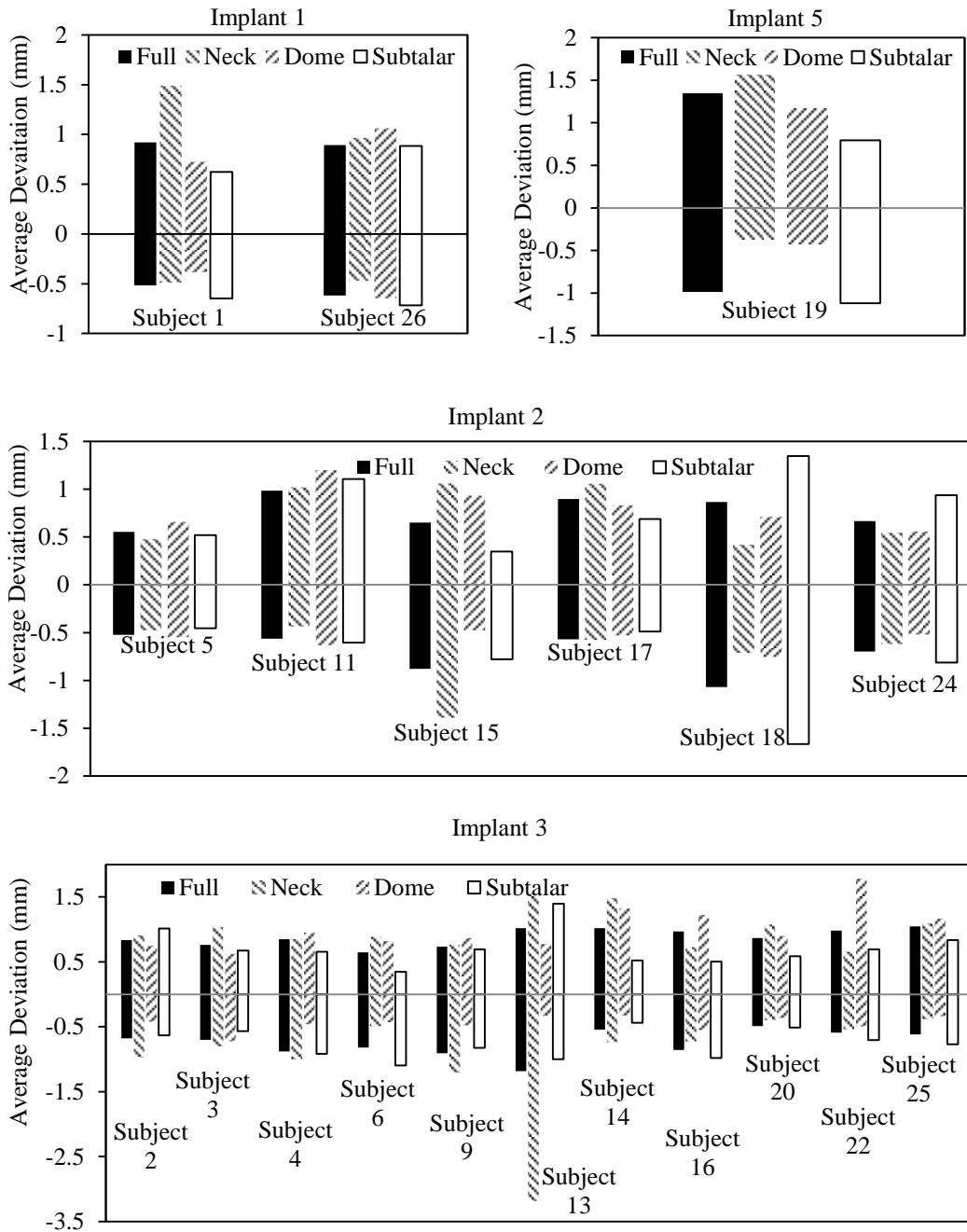
Figure 6: Average Deviation of the different subjects when comparing identical scaled volumes

The average deviations obtained from the 3D deviation analysis after scaling the target models to the reference model are shown in Figure 6. Four target models out of twenty six deviated from the reference model more than ± 1 mm after scaling but the deviation was always less than ± 1.5 mm.

3.3 Verification of Implant sizes

To verify the implant sizes similar deviation analyses were performed on all 27 subjects. Since the articular surface is the prime concern for the success of any joint replacement, therefore, the average deviations between the different implant sizes and the test subjects in the three articular surfaces were estimated, and were found to be less than ± 1.5 mm except five subjects (two subjects deviate in the region of talar neck, two subjects deviate in the region of subtalar region, and one in the talar dome region). The results include the deviation of the whole object

and the three articulating surfaces when compared to the corresponding implant sizes (Figure 7). In most of the cases the average deviations were higher in the talar head region.



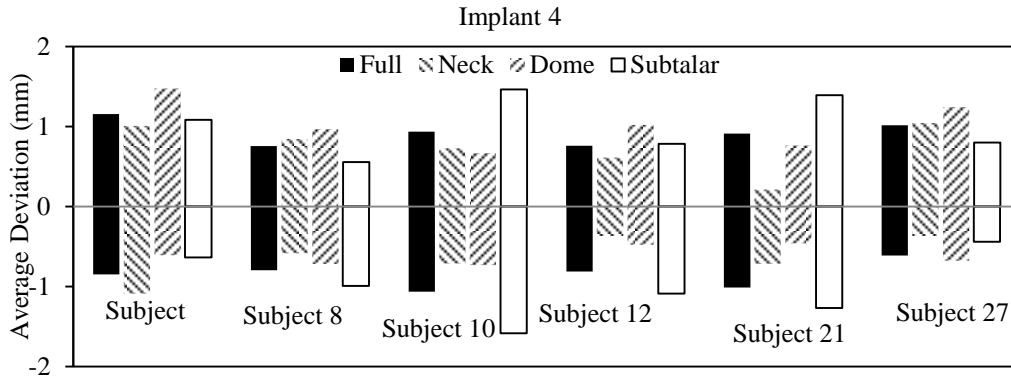


Figure 7: 3D comparison between five implants and twenty seven test subjects

4. Discussions

As discussed in the introduction, the surface topography of the talus bone is complex in nature. Therefore, successful implant design is dependent on the accurate shape matching of the real talus bone which is very challenging. Numerous studies have applied scaling laws on skeletal structures of different animals as well as human models (Parr, Chatterjee, and Soligo 2011; Christiansen 1999; Doube et al. 2009). But all the scaling laws are related to the body weight and cross sectional allometry. However, none of these approaches have been adopted in the current study.

Volume is an important extrinsic property of an object (Griffin 1994). Complex 3D shape is very difficult to analyse and lots of parameters are involved (i.e. cross sectional variation, variation in moment of inertia in three different axes, curvature, length, width and height). However, an object's volume gives a simple measure which eventually represents an object globally.

The present study has investigated the geometric shape variation of the talus bones of different subjects. We utilize the volume of the talus bone for this purpose. Therefore, we only focused on quantifying the volume which is an important parameter for any 3D object analysis. To our best knowledge, this study

is the first to use the volumetric scaling approach to better understand the geometry and surface topography of the talus bones between the subjects.

As the geometric reconstruction method requires some manual detection a first very important step was to analyse the inter-observer reliability. This method proved reliable as the total volume difference was less than 2.5% and the 3D deviation ranged from 0.03-0.26 mm. Analysing the 26 subjects revealed that talus bones are geometrically similar within an average deviation limit of ± 1.5 mm. More subjects are needed to establish the hypothesis that talus bones of the ankle joints are geometrically similar after scaling. The current study focused on the volume of the talus bones. In the future other geometric parameters (e.g. bone length, cross-sectional variation, moment of inertia, curvature of articular surface) will be investigated to verify the geometric similarity of this complex bone.

Another objective of the current study is to generalize and verify the sizes of the talus implants. 3D deviation analyses were performed to fulfill this objective. First it should be noted that the distribution of the subjects into the implants followed a normal distribution in Figure 3. As articulating surfaces are the main area of interest in the biomechanics of joints, therefore, we quantified deviations in three articulating surfaces of the talus bone. Talus bones of two subjects deviate more than ± 1.5 mm from the implants in the region of talar neck, and two subjects deviate more than ± 1.5 mm from the implants in the subtalar region. However, the orthopaedic surgeons may fuse the talar neck to the meta-tarsal. Therefore, higher deviation in the neck region will not be a problematic issue in this perspective.

In this study we found that the deviation is under ± 2 mm. Therefore, another important question for future work is to determine how much deviation can be tolerated clinically. Preliminary work has begun by our group to see the biomechanical effects of using an implant which is either too small or too large for the patient. A detailed numerical analysis on computing the effect of size

variation of the implants on developed mechanical stresses is beyond the scope of this study.

In real time, the volume of fractured talus bone can be obtained from mirroring the contralateral talus bone of the patients. Orthopaedic surgeons need to scan the contralateral ankle joint of the patient to quantify the volume. This will eventually help the surgeons to choose the implant for proper surgical replacement of the damaged talus bone. A similar method has been done for custom talus implant design (Harnroongroj and Vanadurongwan 1997; Magnan, Facci, and Bartolozzi 2004; Stevens et al. 2007). Currently, our research group have found an average dimensional variation of 0.37 mm between left and right ulnas among the same individual (unpublished data). A similar future study will be done on talus.

This study focused on the talus bone of the left foot for all subjects. Currently, we are conducting future work to compare the right to left to verify the similarity whether these five implant sizes will be suitable for the right talus as well. We are also trying to correlate the implant sizes with the body weight which will be a quick way to identify the proper implant size for a specific persons regardless of the talus volume.

The robust and simple technique developed based on the scaling approach in order to design a custom implant for the talus bone was shown to be very promising. The cubic root of the difference in volume was shown to be a reliable method in choosing the proper implant size for a person with a damaged talus. To the author's best knowledge this stands as the first attempt to develop a process to design a set of talar body implants which might be applicable for all patients. Literature on geometric and morphometric analysis of talus bone is scarce, and no such study was done so far on the different implant sizes of talus bones. Therefore, we did not get any direct comparison which supports our study. It is to be noted that we assume the reference (Subject Id 28) model picked in this study

didn't have any irregularity. In future studies an approach to obtain an average shape for template creation will be adopted.

5. Conclusions

The current study focused on the geometric similarity and generalisation of talus implants utilizing the whole geometry of the talus bone. Although the talus bones were different in size, however, we found geometric similarity between them within certain range of deviation. Our method was reliable as it had small inter-observation variation. In this study, we also have demonstrated a generalized procedure of template creation using the geometric topography of the talus bone. The results presented in this study showed that the proposed five standard sizes of implants exhibited satisfactory results in terms of deviation. Although, clinically articulating surfaces are the prime concern during any surgical implantation, therefore, we also performed deviation analysis on the three main articulating surfaces of the talus bone. Proper articulation will not only minimize wear and tear of the articular cartilage, but also ensure joint conformity. Our works showed excellent results (i.e., average deviation less than or equal to 2 mm) on these three articulating surfaces. Future works need to be done to determine the deviation threshold before having a negative clinical effect on the patients. Future work will also investigate the size variation of the talus implant and the choice of proper materials for implant design.

Conflict of interest statement:

The Authors have no conflict of interest to declare.

Acknowledgements:

This research work was partially supported by the Natural Sciences and Engineering Research Council (NSERC) of Canada. We are thankful to Dr. Suki Dhillon for collecting the experimental data.

References

- Akiyama, K, T Sakai, N Sugimoto, H Yoshikawa, and K Sugamoto. 2012. "Three-dimensional Distribution of Articular Cartilage Thickness in the Elderly Talus and Calcaneus Analyzing the Subchondral Bone Plate Density." *Osteoarthritis and Cartilage / OARS, Osteoarthritis Research Society* 20 (4) (April): 296–304. doi:10.1016/j.joca.2011.12.014.
- Andrea Hayes, B. S. E., M. D. YukiTochigi, and L. S. Charles. 2012. "ANKLE MORPHOMETRY ON 3D-CT IMAGES" (July 30).
<http://www.uiortho.com/ioj/2006/hayesankle.pdf>.
- Barton, Tristan, Francois Lintz, and Ian Winson. 2011. "Biomechanical Changes Associated with the Osteoarthritic, Arthrodesed, and Prosthetic Ankle Joint." *Foot and Ankle Surgery* 17 (2) (June): 52–57.
doi:10.1016/j.fas.2011.01.010.
- Bažant, Zdenek P. 2005. *Scaling of Structural Strength, Second Edition*. 2nd ed. Butterworth-Heinemann.
- Bažant, Zdeněk P. 1984. "Size Effect in Blunt Fracture: Concrete, Rock, Metal." *Journal of Engineering Mechanics* 110 (4) (April): 518–535.
doi:10.1061/(ASCE)0733-9399(1984)110:4(518).
- Berlet, G C, T H Lee, and E G Massa. 2001. "Talar Neck Fractures." *The Orthopedic Clinics of North America* 32 (1) (January): 53–64.
- Carpinteri, Alberto, and Bernardino Chiaia. 1997. "Multifractal Scaling Laws in the Breaking Behaviour of Disordered Materials." *Chaos, Solitons & Fractals* 8 (2) (February): 135–150. doi:10.1016/S0960-0779(96)00088-4.

- Carpinteri, Alberto, and Nicola Pugno. 2005. "Are Scaling Laws on Strength of Solids Related to Mechanics or to Geometry?" *Nature Materials* 4 (6) (June): 421–423. doi:10.1038/nmat1408.
- Christiansen, P. 1999. "Scaling of the Limb Long Bones to Body Mass in Terrestrial Mammals." *Journal of Morphology* 239 (2) (February): 167–190. doi:10.1002/(SICI)1097-4687(199902)239:2<167::AID-JMOR5>3.0.CO;2-8.
- Conti, S F, and Y S Wong. 2001. "Complications of Total Ankle Replacement." *Clinical Orthopaedics and Related Research* (391) (October): 105–114.
- Daniels, T R, and J W Smith. 1993. "Talar Neck Fractures." *Foot & Ankle* 14 (4) (May): 225–234.
- Doube, Michael, Alexis Wiktorowicz Conroy, Per Christiansen, John R. Hutchinson, and Sandra Shefelbine. 2009. "Three-Dimensional Geometric Analysis of Felid Limb Bone Allometry." *PLoS ONE* 4 (3) (March 9): e4742. doi:10.1371/journal.pone.0004742.
- Fessy, M. H., J. P. Carret, and J. Béjui. 1997. "Morphometry of the Talocrural Joint." *Surgical and Radiologic Anatomy* 19 (5): 299–302. doi:10.1007/BF01637597.
- Fortin, P T, and J E Balazsy. 2001. "Talus Fractures: Evaluation and Treatment." *The Journal of the American Academy of Orthopaedic Surgeons* 9 (2) (April): 114–127.
- Glazebrook, Mark, Tim Daniels, Alastair Younger, C J Foote, Murray Penner, Kevin Wing, Johnny Lau, Ross Leighton, and Michael Dunbar. 2008. "Comparison of Health-related Quality of Life Between Patients with End-stage Ankle and Hip Arthrosis." *The Journal of Bone and Joint Surgery. American Volume* 90 (3) (March): 499–505. doi:10.2106/JBJS.F.01299.
- Griffin, L D. 1994. "The Intrinsic Geometry of the Cerebral Cortex." *Journal of Theoretical Biology* 166 (3) (February 7): 261–273. doi:10.1006/jtbi.1994.1024.
- Harnroongroj, T., and V. Vanadurongwan. 1997. "The Talar Body Prosthesis*." *The Journal of Bone and Joint Surgery (American)* 79 (9): 1313–22.

- Huang, Peng-Ju, and Yuh-Min Cheng. 2005. "Delayed Surgical Treatment for Neglected or Mal-reduced Talar Fractures." *International Orthopaedics* 29 (5): 326–329. doi:10.1007/s00264-005-0675-1.
- Inokuchi, S, K Ogawa, and N Usami. 1996. "Classification of Fractures of the Talus: Clear Differentiation Between Neck and Body Fractures." *Foot & Ankle International / American Orthopaedic Foot and Ankle Society [and] Swiss Foot and Ankle Society* 17 (12) (December): 748–750.
- Kakkar, Rahul, and M.S. Siddique. 2011. "Stresses in the Ankle Joint and Total Ankle Replacement Design." *Foot and Ankle Surgery* 17 (2) (June): 58–63. doi:10.1016/j.fas.2011.02.002.
- Kenwright, J., and R. G. Taylor. 1970. "MAJOR INJURIES OF THE TALUS." *Journal of Bone & Joint Surgery, British Volume* 52-B (1) (February 1): 36–48.
- Leardini, A. 2001. "Geometry and Mechanics of the Human Ankle Complex and Ankle Prosthesis Design." *Clinical Biomechanics (Bristol, Avon)* 16 (8) (October): 706–709.
- Leardini, Alberto. 2001. "Geometry and Mechanics of the Human Ankle Complex and Ankle Prosthesis Design." *Clinical Biomechanics* 16 (8) (October): 706–709. doi:10.1016/S0268-0033(01)00022-5.
- Lesic, Aleksandar, and Marko Bumbasirevic. 2004. "Ankle Fractures." *Current Orthopaedics* 18 (3) (June): 232–244. doi:10.1016/j.cuor.2004.03.001.
- Magnan, B., E. Facci, and P. Bartolozzi. 2004. "Traumatic Loss of the Talus Treated with a Talar Body Prosthesis and Total Ankle Arthroplasty A Case Report." *The Journal of Bone and Joint Surgery (American) Case Reports* 86 (8): 1778–1782.
- MANTER, J T. 1946. "Distribution of Compression Forces in the Joints of the Human Foot." *The Anatomical Record* 96 (3) (November): 313–321.
- Miller, C E, C Basu, G Fritsch, T Hildebrandt, and J R Hutchinson. 2008. "Ontogenetic Scaling of Foot Musculoskeletal Anatomy in Elephants." *Journal of the Royal Society, Interface / the Royal Society* 5 (21) (April 6): 465–475. doi:10.1098/rsif.2007.1220.

- Müller, R, M Hahn, M Vogel, G Delling, and P Rügsegger. 1996. "Morphometric Analysis of Noninvasively Assessed Bone Biopsies: Comparison of High-resolution Computed Tomography and Histologic Sections." *Bone* 18 (3) (March): 215–220.
- Parr, William C H, Helen J Chatterjee, and Christophe Soligo. 2011. "Inter- and Intra-specific Scaling of Articular Surface Areas in the Hominoid Talus." *Journal of Anatomy* 218 (4) (April): 386–401. doi:10.1111/j.1469-7580.2011.01347.x.
- Salathé, E P, Jr, G A Arangio, and E P Salathé. 1986. "A Biomechanical Model of the Foot." *Journal of Biomechanics* 19 (12): 989–1001.
- Santavirta, S, S Seitsalo, O Kiviluoto, and P Myllynen. 1984. "Fractures of the Talus." *The Journal of Trauma* 24 (11) (November): 986–989.
- van Schaik, J J, H Verbiest, and F D van Schaik. 1985. "Morphometry of Lower Lumbar Vertebrae as Seen on CT Scans: Newly Recognized Characteristics." *AJR. American Journal of Roentgenology* 145 (2) (August): 327–335.
- Seth, Ajai. 2011. "A Review of the STAR Prosthetic System and the Biomechanical Considerations in Total Ankle Replacements." *Foot and Ankle Surgery: Official Journal of the European Society of Foot and Ankle Surgeons* 17 (2) (June): 64–67. doi:10.1016/j.fas.2011.02.003.
- Stagni, Rita, Alberto Leardini, Fabio Catani, and Angelo Cappello. 2004. "A New Semi-automated Measurement Technique Based on X-ray Pictures for Ankle Morphometry." *Journal of Biomechanics* 37 (7) (July): 1113–1118. doi:10.1016/j.jbiomech.2003.11.017.
- Stagni, Rita, Alberto Leardini, Andrea Ensini, and Angelo Cappello. 2005. "Ankle Morphometry Evaluated Using a New Semi-automated Technique Based on X-ray Pictures." *Clinical Biomechanics* 20 (3) (March): 307–311. doi:10.1016/j.clinbiomech.2004.11.009.
- Stevens, Benjamin W., Christopher M. Dolan, John G. Anderson, and Charles D. Bukrey. 2007. "Custom Talar Prosthesis After Open Talar Extrusion in a

Pediatric Patient.” *Foot & Ankle International* 28 (8) (August): 933–938.
doi:10.3113/FAI.2007.0933.

Sugimoto, Kazuya, Yoshinori Takakura, Yoshiyuki Tohno, Tsukasa Kumai, Kenji Kawate, and Kunihiro Kadono. 2005. “Cartilage Thickness of the Talar Dome.” *Arthroscopy: The Journal of Arthroscopic & Related Surgery: Official Publication of the Arthroscopy Association of North America and the International Arthroscopy Association* 21 (4) (April): 401–404.
doi:10.1016/j.arthro.2004.12.005.

Tanaka, Yasuhito, Yoshinori Takakura, K. Kadono, Akira Taniguchi, K. Hayashi, Jin Iida, Koh Ichi Sugimoto, Yasuaki Tohma, and Hajime Ohgushi. 2003. “Alumina Ceramic Talar Body Prosthesis for Idiopathic Aseptic Necrosis of the Talus.” *Key Engineering Materials* 240-242: 805–808.
doi:10.4028/www.scientific.net/KEM.240-242.805.

West, Geoffrey B., and James H. Brown. 2004. “Life’s Universal Scaling Laws” *Physics Today* 57 (9): 36–42. doi:10.1063/1.1809090.

West, Geoffrey B., James H. Brown, and Brian J. Enquist. 1999. “The Fourth Dimension of Life: Fractal Geometry and Allometric Scaling of Organisms.” *Science* 284 (5420) (June 4): 1677–1679.
doi:10.1126/science.284.5420.1677.

Chapter 4: Summary and Conclusions

The major novelty and strength of this research is the utilization of the geometric shape of the load-bearing joints to quantify the “geometric” differences between healthy and symptomatic joints of different individuals.

One of our objectives is to utilize the geometric shape of the PF joints to investigate the PFPS. Most of the studies on the PFPS are concerned with the lateral malalignment/maltracking of the patella, and clinical treatments are aimed towards fixing the malalignment/maltracking through strengthening the vastus medialis (VM) muscle. According to the agreed upon clinical diagnosis, the weakness of the vastus medialis compared to the vastus lateralis is the usual muscle force imbalance which causes lateral tilt/shift of the patella leading to PFPS. However, our study showed completely reversed trend which was not reported in the previous studies. We found higher stresses in the medial side of the symptomatic PF joints which might cause medial pain. If this is the situation, then, the current treatment strategy could be harmful for medial maltracker groups. However, more subjects are needed in the future to verify the findings.

Another objective of the current study is to analyse the geometric shape of the talus bone to standardize the sizing of the talus bone implants for talus bone replacement surgery. To fulfill this objective, we analysed twenty seven different intact talus bones. We reported that talus bones of the ankle joints are geometrically similar. Furthermore, we proposed five different talus implant sizes for talar body replacement surgery based on the criteria developed.

Fracturing of the talus bone in the ankle joint can occur for various reasons. In addition, fracturing of this bone is associated with high and abnormal compressive forces. Replacement of the talus bone with an implant is a possible solution, and in this case restoring proper ankle function depends primarily on the proper choice of implant. A mismatch in the implant choice will not only increase the

stress on the articulating surfaces but will also create long-term detrimental effects on proper ankle motion. The present results of the geometric analysis of the talus bone have shown that the five implant sizes will be very promising during talus bone replacement surgery. This study does entail certain limitations. We only focused on the right ankle. Future study will investigate whether these five implant sizes will be applicable for left ankles or not. Future work will also investigate the size variation of the talus implant and the choice of proper materials for implant design.

Improper matching of implants compared to the actual bone could, not only increase the contact stress, but also increase the possibility of failure of the implant in the long term. To date, the choice of implant for talus bone replacement has depended on the radiographic image of the bone, the patient's condition, what implant sizes are available, as well as the surgeon's experience. To the author's best knowledge no study has been performed to investigate the effect on the patient after surgery based on the size of the given implant. Patient-specific implant design is not practical due to time constraints, market unavailability of the proper implant size, as well as the possible need for immediate surgery depending on the severity of the injury. It is therefore necessary to investigate whether the surgeons opt for an available larger size or a smaller size of implant for surgery. FEA can play an important role in analyzing and predicting the outcome of the talus bone replacement with an implant after surgery. Until now, there has been no such study to investigate the effect of imperfections of the talus implant on the ankle joint. Currently we are conducting FEA to investigate the influence of different sizes of custom-made talus implants on the contact characteristics of the ankle joint.

Biography

Kamrul Islam was born on 14th December, 1986 in Dhaka, Bangladesh. He graduated from Bangladesh University of Engineering and Technology (BUET) in 2009 with a specialization in Structural Engineering. After his graduation, he joined in the Military Institute of Science and Technology (MIST) as a lecturer in January 2010, and served as a faculty member in the Structural division for eight months. In the same year (fall 2010), he started his M.Sc. at the University of Alberta in Structural Engineering. Kamrul is highly passionate about teaching and he enjoyed teaching more than anything. He is interested in pursuing PhD in Structural-Biomechanical Engineering to further continue his research to fulfill his dream to go into Academia.